



HAL
open science

Pb-free halide perovskites for solar cells, light-emitting diodes, and photocatalysts

Pingping Jiang, Debdipto Acharya, George Volonakis, Marios Zacharias, Mikaël Kepenekian, Laurent Pedesseau, Claudine Katan, Jacky Even

► **To cite this version:**

Pingping Jiang, Debdipto Acharya, George Volonakis, Marios Zacharias, Mikaël Kepenekian, et al.. Pb-free halide perovskites for solar cells, light-emitting diodes, and photocatalysts. *APL Materials*, 2022, 10 (6), pp.060902. 10.1063/5.0095515 . hal-03694654

HAL Id: hal-03694654

<https://hal.science/hal-03694654v1>

Submitted on 13 Jun 2022

HAL is a multi-disciplinary open access archive for the deposit and dissemination of scientific research documents, whether they are published or not. The documents may come from teaching and research institutions in France or abroad, or from public or private research centers.

L'archive ouverte pluridisciplinaire **HAL**, est destinée au dépôt et à la diffusion de documents scientifiques de niveau recherche, publiés ou non, émanant des établissements d'enseignement et de recherche français ou étrangers, des laboratoires publics ou privés.


Pb-free halide perovskites for solar cells, light-emitting diodes, and photocatalysts F

Cite as: APL Mater. 10, 060902 (2022); <https://doi.org/10.1063/5.0095515>

Submitted: 11 April 2022 • Accepted: 19 May 2022 • Published Online: 10 June 2022

 Pingping Jiang, Debdipto Acharya,  George Volonakis, et al.

COLLECTIONS

 This paper was selected as Featured



View Online



Export Citation



CrossMark

ARTICLES YOU MAY BE INTERESTED IN

[Mechanism of Mn emission: Energy transfer vs charge transfer dynamics in Mn-doped quantum dots](#)

APL Materials 8, 020901 (2020); <https://doi.org/10.1063/1.5140888>

[Insights into the charge carrier dynamics in perovskite/Si tandem solar cells using transient photocurrent spectroscopy](#)

Applied Physics Letters 120, 173504 (2022); <https://doi.org/10.1063/5.0080109>

[Hydroxymethyl PEDOT microstructure-based electrodes for high-performance supercapacitors](#)

APL Materials 10, 061101 (2022); <https://doi.org/10.1063/5.0088452>

APL Materials

Special Topic: Design and Development of High Entropy Materials

Submit Today!











Pb-free halide perovskites for solar cells, light-emitting diodes, and photocatalysts

Cite as: APL Mater. 10, 060902 (2022); doi: 10.1063/5.0095515

Submitted: 11 April 2022 • Accepted: 19 May 2022 •

Published Online: 10 June 2022



Pingping Jiang,¹  Debdipto Acharya,¹  George Volonakis,²  Marios Zacharias,¹  Mikaël Kepenekian,² 
Laurent Pedesseau,¹  Claudine Katan,²  and Jacky Even^{1,a)} 

AFFILIATIONS

¹Univ Rennes, INSA Rennes, CNRS, Institut FOTON-UMR 6082, F-35000 Rennes, France

²Univ Rennes, ENSCR, INSA Rennes, CNRS, ISCR-UMR 6226, F-35000 Rennes, France

^{a)}Author to whom correspondence should be addressed: jacky.even@insa-rennes.fr

ABSTRACT

Metal halide perovskites have recently emerged as one of the most promising classes of semiconductors for various applications, especially in the field of optoelectronics. Lead-based halide perovskite materials, virtually unexploited for decades, have become prominent candidates due to their unique and intrinsic physicochemical and optical properties. Current challenges faced by the scientific community to capitalize on the properties of Pb-based perovskites are mainly associated with environmental concerns due to the toxicity of Pb and their poor stability. Under this context, over recent years, a number of new Pb-free halide perovskite (and perovskite-like) semiconductor classes have been introduced. This Perspective reviews recent developments in Pb-free halide perovskites, which specifically target their application in solar cells, light-emitting devices, and photocatalysts. Each type of Pb-free material is paired with a specific optoelectronic application, and the latest record performances are reported. Although these materials do not yet exhibit as attractive intrinsic optoelectronic properties as the Pb-based halide perovskites, their potential as alternatives for well-suited applications is discussed.

© 2022 Author(s). All article content, except where otherwise noted, is licensed under a Creative Commons Attribution (CC BY) license (<http://creativecommons.org/licenses/by/4.0/>). <https://doi.org/10.1063/5.0095515>

I. INTRODUCTION

For the past decade, halide perovskite semiconductors have received tremendous attention due to their tunable bandgaps, impressive optoelectronic properties, ease of process, and low fabrication cost, all of which lead to an ever-expanding range of potential device applications.¹ This applies especially to their exploitation as solar cells, light-emitting diodes, photocatalysts, as well as various photodetectors.^{1–4} 3D hybrid halide inorganic perovskites are ionic semiconductors typically composed of lead (Pb²⁺), halogen anions (X⁻ = I⁻, Br⁻, Cl⁻), and small organic cations or cesium (Cs⁺). In 2009, MAPbI₃ (MA = CH₃NH₃⁺, methylammonium) and MAPbBr₃ were the first perovskites successfully applied as photovoltaic materials in a solar cell.⁵ MAPbI₃ exhibits remarkable properties for solar cell applications, such as a sharp optical absorption with a large absorption coefficient of 10⁴ cm⁻¹ and a bandgap of 1.5–1.6 eV, as evaluated by UV photoelectron or optical spectroscopy.⁶ Moreover, MAPbI₃ single crystals present ultra-low trap densities, namely,

10⁹–10¹⁰ traps per cm³, and sizable charge carrier diffusion lengths ranging within 3–10 μm.^{7,8}

The structural, thermodynamic, and electronic properties of Pb-based halide perovskites can be tuned by substituting MA with other cations, such as Cs⁺, K⁺, and FA [FA = HC(NH₂)₂⁺, formamidinium], and/or their mixtures. For example, by replacing MA with a suitable mixture of FA and Cs⁺, the materials' stability increases and the bandgap decreases by 0.07 eV.⁹ Mixing halogen atoms to form mixed-halide perovskites is another efficient way of tuning the bandgap and spanning the absorption and emission energies over the UV–visible to near IR regions. Therefore, 3D halide perovskites with finely tuned Pb-based alloys of both cations and halogens are ideal for high performance solar cells, including tandems on silicon. To date, the highest certified Power Conversion Efficiency (PCE) of a Pb-based perovskite solar cell is 25.8%. This recent record was achieved, thanks to the insertion of a Cl-based coherent interlayer between the FAPbI₃ and the SnO₂ electrode.¹⁰

Despite the remarkable performance of Pb-based halide perovskites, the materials' stability under ambient conditions and the environmental concerns raised over the presence of Pb remain active challenges toward their large-scale application and commercialization.^{11–15} Various strategies are developed to overcome these hindrances. By device or module encapsulation, the halide perovskite materials can be indeed nicely protected from exposure to moisture, UV light, heating, or air, thus mitigating the fast degradation for their long-lasting purpose.^{16,17} On the other hand, Pb-free perovskites as well as materials derived from the perovskite structure (also called perovskite-like structures or perovskitoids), as introduced in Sec. II, are explored with the aim to obtain similar or even better properties than standard Pb-based materials.¹⁸ In this Perspective, we discuss how Pb-free perovskites or perovskite-like semiconductors are used for specific optoelectronic devices, namely, solar cells, light-emitting diodes, and photocatalysts. Other explored applications include memristors, transistors, lasers, photodetectors, and various sensors.¹⁹ Section II presents a classification of Pb-free materials, then we list and compare, for the best suited applications, the record performances reported so far for each class.

II. TYPES OF LEAD-FREE PEROVSKITES

The cubic ABX_3 perovskite structure within the $Pm\bar{3}m$ space group is the reference perovskite structure. It consists of a network of corner-sharing BX_6 octahedra, with the A-site atom sitting in the cuboctahedral cavity formed in between the octahedra, as shown in Fig. 1. For typical halide perovskites, a monovalent organic or inorganic cation occupies the A-site, a divalent (2+) metal, most notably Pb, is at the B-site, and the halogen anion is at the X-site. Within the lattice, A-site atoms typically only have indirect effects on the electronic structure of the materials, as the electronic states of the typical A-site cations (i.e., Cs, MA, and FA) are far from the band edges. Yet, these atoms can induce structural modifications, which in turn can lead to modifications of their electronic structure and the exhibited bandgaps. Akkerman and Manna²⁰ have recently categorized different structure types of materials based on the three- and two-dimensional (3D and 2D) ordered structures, as derived from the reference ABX_3 lattice. Here, we summarize materials that are substitutionally engineered at the B-site so that all Pb atoms are replaced, only including those that have been applied in optoelectronic devices to date.

First, as Sn^{2+} and Ge^{2+} share the same nominal oxidation state with Pb, Sn- and Ge-based perovskite materials can attain the same ABX_3 stoichiometry. The formed conventional $A(Sn,Ge)X_3$ perovskite structures can adopt either the cubic reference lattice, like their Pb-based counterparts, or slightly distorted ones due to the constituents' incorporation. Moreover, since Sn, Ge, and Pb belong to the same column of the Periodic Table, they share the same electronic configuration (valency); thus, Sn and Ge-based perovskites are most likely to exhibit similar electronic and optical properties as their Pb-based counterparts. In fact, the remarkable physical and optoelectronic properties of $APbX_3$ perovskites are known to directly relate to the antibonding electronic states: $Pb[6s]-X[np]$ and $Pb[6p]-X[np]$ (with $n = 3, 4,$ and 5 for $X = Cl, Br,$ and I) located at the valence band maximum (VBM) and conduction band minimum (CBM), respectively.²¹

A set of popular examples of Sn-based perovskites are $CsSnI_3$, $MASnI_3$, and $FASnI_3$, all of which have direct optical bandgaps in the range of 1.3–1.4 eV.^{18–20} The electronic structure of these materials shows that the band-dispersion is similar to the Pb-based compounds, while their bandgaps are ideally placed for photovoltaic devices in the near-infrared range.^{22,23} Yet, a well-known drawback of Sn-based perovskites is the favored oxidation of Sn^{2+} to Sn^{4+} , leading to a natural *p*-doping in samples but also to an irreversible degradation of the device performances over a short period.^{24,25} In addition, the ease of formation of Sn vacancies results in an electrical behavior close to a metal that is far from ideal for the reproducibility, stability, and performance of devices. Therefore, the incorporation of excess Sn^{2+} in the compounds and the use of large cations are recommended in order to suppress the unwanted defects- or traps-induced recombination.^{26,27} We note that extra care should be taken when large cations are introduced, usually to avoid disrupting the pristine crystal structure, as the materials can then form one-dimensional networks of octahedra, like in the case of $(CH_3)_3SSnI_3$.²⁸ Another class of materials with enhanced stability is obtained by adding large ethylenediammonium (en) cations within the $ASnI_3$ perovskite lattice ($A = MA, FA$) to form the well-known hollow perovskite lattices.²⁹

Second, classic Ge-based perovskites are $CsGeI_3$, $MAGeI_3$, and $FAGeI_3$, exhibiting direct bandgaps of 1.6, 1.9, and 2.2 eV, respectively.³⁰ Similar to the Sn-based perovskites, Ge-based ones also face stability issues due to the oxidation of Ge^{2+} to Ge^{4+} . In addition, the octahedra in Ge^{2+} based perovskites are typically heavily distorted due to the stereochemical expression of the Ge lone pair.³⁰

Another approach toward stable and performant materials is alloying. Such an alloying strategy has been first explored for the case of mixing Pb with Sn.³¹ These Pb/Sn mixed alloys have a smaller bandgap compared to the pristine compounds. Recently, this strategy has been expanded to fully Pb-free materials by alloying Ge with Sn, which were found to exhibit higher stabilities and narrower bandgaps than the pristine Sn and Ge-based materials, with $CsSn_{0.5}Ge_{0.5}I_3$, for example, exhibiting an optical bandgap of 1.5 eV.³² Similar to the case of Pb-based materials, the design of 2D/3D heterostructures is another promising recipe for achieving highly efficient and stable Sn-based solar cells. Specifically, forming well-aligned 2D layers over the 3D crystal phase can considerably improve the hysteresis and light soaking of the compounds. As a consequence, the charge carrier collection, device stability, and efficiency improve with respect to the pristine 3D material.^{33,34} Yet, the device performance of Sn and Ge based perovskites is still far from those of the Pb based counterparts, and this brings forward the indispensability of more endeavors.

Another class of materials that have been derived from the ABX_3 perovskite lattice is the so-called "halide double perovskites." Many compounds have been reported since the early 1970s, often referred to as elpasolites,³⁵ and exhibit large bandgaps particularly prominent for scintillating applications. Over the past few years, a series of new halide double perovskites with relatively low bandgaps have been synthesized as possible Pb-free alternatives for optoelectronics.^{36–42} These double perovskites keep the conventional 3D perovskite structure, but every two B^{2+} site cations are substituted by two cations B and B' with formal oxidation states of +3 and +1, as shown in Fig. 1.^{36–38,43} The double perovskite structure corresponds to a general chemical formula of

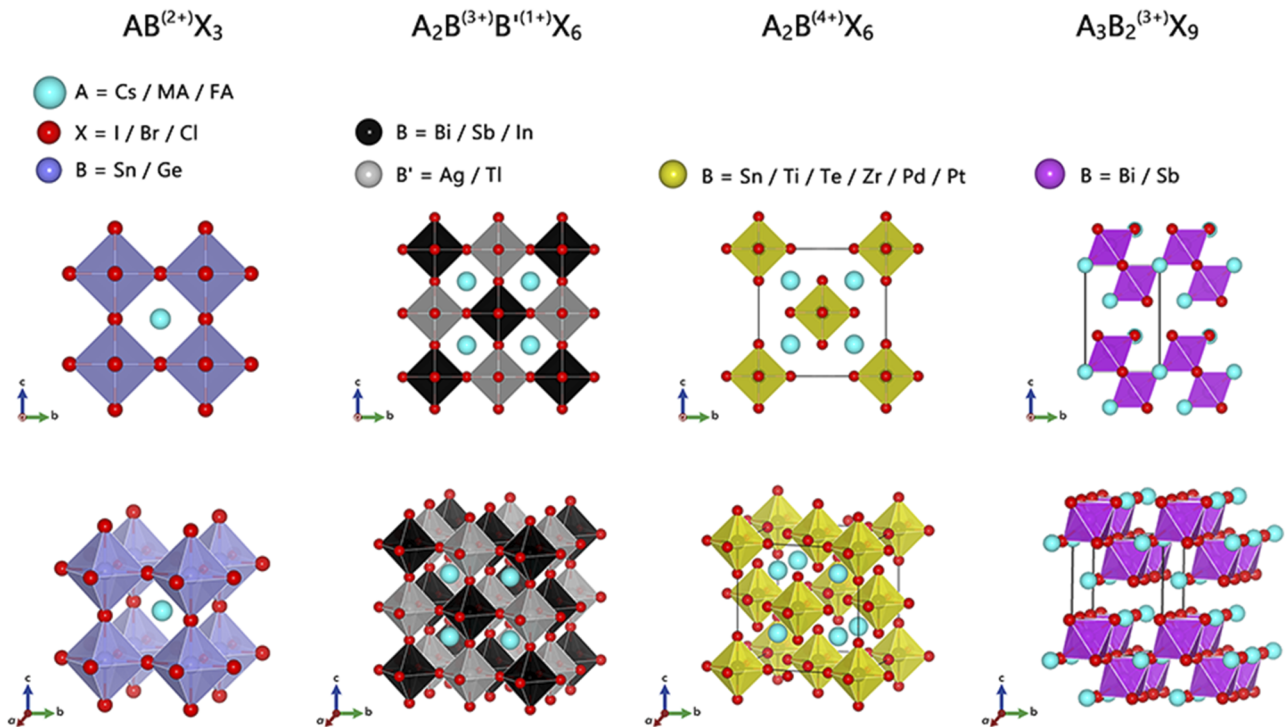


FIG. 1. Structure of the conventional types of Pb-free metal halide perovskites. $AB(2+)X_3$ perovskites (with B = Sn/Ge), $A_2B(3+)B'(1+)X_6$ double perovskites (with B = Bi/Sb/In and B' = Ag/Tl), $A_2B(4+)X_6$ vacancy ordered double perovskites (with B = Sn/Ti/Te/Zr/Pd/Pt), and $A_3B_2(3+)X_9$ 2D layered perovskite (with B = Bi/Sb). A-site atoms can be Cs, MA, FA, and their combinations, while at the X-site, I, Br, Cl, and their combinations. Atoms A and X are in cyan and red, respectively, and atoms B or B' in four different classes are shown as octahedra.

$A_2BB'X_6$, which is simply obtained by doubling the standard ABX_3 perovskite lattice. Halide double perovskites typically crystallize in face-centered cubic $Fm\bar{3}m$ space groups at room temperature and are known to form stable crystals under ambient conditions.^{37,38,44} To date, the two of the most successful halide double perovskites are $Cs_2AgBiBr_6$ ^{37,38} and $Cs_2AgInCl_6$,³² which have attracted much interest for optoelectronic applications as the former exhibits one of the smallest bandgaps within the halide double perovskites class (estimated at 1.95 eV³⁶), and the latter exhibits interesting emission properties, attaining record-high photoluminescence quantum yield (PLQY) values upon appropriate doping.⁴⁴ Another series of low bandgap double perovskite materials that have been proposed are the ones containing Tl^+ instead of Ag^+ .^{45–47} Noteworthy, besides halide perovskites, low bandgap oxide perovskites, such as Ba_2AgIO_6 and Ba_2AuIO_6 , which contain heptavalent iodine at the B'-site, are also explored as promising candidates for optoelectronics.^{48,49} Another class of materials that have emerged as potentially interesting low bandgap perovskites are the so-called 111-oriented layered double perovskites. $Cs_4CuSb_2Cl_{12}$ was first reported by Vargas *et al.*,⁵⁰ and there has been an increased interest in the class⁵¹ and other lead-free derivatives synthesized, such as $Cs_4CuIn_2Cl_{12}$ and $Cs_4Cd_{1-x}Mn_xBi_2Cl_{12}$.^{52,53}

Starting from the $A_2BB'X_6$ double perovskite lattice, a different class of materials can be defined by replacing the B' site with vacancies, and the B-site with a suitably charged metal to maintain

charge neutrality. These compounds are known as vacancy ordered double perovskites (A_2BX_6), such as Cs_2SnI_6 and Cs_2TiBr_6 . Similar to double perovskites, the A_2BX_6 lattice can be derived from the conventional perovskites by doubling the ABX_3 unit cell along all three crystallographic axes but subsequently removing every other B site cation. This vacancy ordered lattice is shown in Fig. 1, and typically the materials share the same $Fm\bar{3}m$ space group as double perovskites. Interestingly, by exposing the single ABX_3 perovskite $CsSnI_3$ to air, it can transform to the vacancy ordered Cs_2SnI_6 state by the oxidation of Sn^{2+} to Sn^{4+} .⁵⁴ Compared to the conventional ABX_3 , A_2BX_6 compounds typically possess longer B–X bonds, lower defect density, and better stability under ambient conditions. Despite being made by structurally isolated BX_6 octahedra, therefore, exhibiting low structural and electronic dimensionality, some of the materials have surprisingly dispersive electronic bands and low electronic bandgaps. For example, Cs_2SnI_6 has an optical bandgap of just about 1.3 eV,^{55,56} very close to cubic $CsSnI_3$, and a dispersive conduction band.⁵⁷ Moreover, vacancy ordered halide double perovskites with Pt, Pd, Te, Ti, and Zr as the trivalent atom in the center of the octahedron have been shown to also form stable compounds and exhibit bandgaps within the near infrared.^{57–62}

Finally, the concept of vacancy ordering can be expanded to cover another type of Pb-free materials that contain two trivalent cations that replace three Pb^{2+} atoms. The lattice of $A_3B_2X_9$ can

be considered as a tripled ABX_3 perovskite structure that contains one vacancy to maintain charge neutrality. In the lattice, as shown in Fig. 1, the vacancies are ordered along the (111) plane, making 2D layers of BX_6 octahedra that crystallize usually in a trigonal $P\bar{3}m1$ space group. These structures have been also referred to as “2D layered perovskite derivatives” and some examples of materials are $Cs_3Bi_2Br_9$ and $Cs_3Sb_2Br_9$.^{63,64} However, within the same $A_3B_2X_9$ stoichiometry compounds, notably $Cs_3Bi_2I_9$ ⁶⁵ form another perovskitoid structure, within which the octahedra are face-sharing typically attaining a hexagonal $P6_3/mmc$ space-group at room temperature. In the following, we include all $A_3B_2X_9$ materials that have been employed in optoelectronic applications, as in some cases, materials like $Cs_3Sb_2I_9$ and $Cs_3Bi_2I_9$ ^{66,67} can attain both structures. These $A_3B_2X_9$ Pb-free halide perovskites contain a pnictogen atom as the trivalent cation at the octahedra center (i.e., Sb and Bi) and are known to exhibit excellent air stability with their bandgaps ranging between 1.9 and 2.9 eV.^{68,69}

Overall, we have summarized the structural details of the four typical prototype lattices, as shown in Fig. 1, which have been applied to date in manufacturing Pb-free optoelectronic devices. In Secs. III–V, we will overview their device performances and characteristics and highlight the emerging trends within each type of the targeted applications: solar cells, light emitters, and photocatalysts.

III. SOLAR CELLS

Perovskite photovoltaics is the fastest ever-growing photovoltaic technology, with great potential to open the door for low-cost and efficient solar cells. This is a direct consequence of the almost perfect electronic and optical properties of Pb-based perovskites for solar cell applications. Starting from 2009, when $MAPbI_3$ was first used as a light-sensitizer with a PCE of 3.8%,⁵ halide perovskite solar cells have made a major step forward in 2012 by using $MAPbI_3$ films and achieved a PCE of around 10%.^{70–72} Interestingly, at the same period, the 3D Pb-free perovskite $CsSnI_3$ was successfully used as a hole-conducting layer in an efficient dye-sensitized solar cell.⁶⁰ To date, the highest published PCE for a Pb-based perovskite solar cell is 25.8%¹⁰ (certified 25.5%) obtained from the cooperation between South Korean laboratories from the Ulsan National Institute of Science and Technology (UNIST) and the Pohang Accelerator Laboratory (PAL). Furthermore, it is demonstrated that perovskite solar cells can be efficiently combined with silicon cells in tandem architectures, approaching PCE of 30% and able to overcome the performances of both separated technologies. The current certified record of 29.8% has been achieved by Helmholtz Zentrum Berlin.⁷³

Yet, Pb-based solar cells face major stability issues, which can be at least partly tackled by considering 2D Pb-based perovskites with optimized cell configurations and device encapsulations.^{74,75} Similar strategies are not yet fully explored for Pb-free perovskite technologies. Moreover, additives specifically dedicated to Pb-free materials may bring interesting improvements in device stability and performance. For example, SnF_2 ,²⁶ GeI_2 ,⁷⁶ or organic compounds^{27,77} dissolved in the precursor solution contribute to the perovskite film quality, reducing surface defects/traps, attaining better crystallinity, and most importantly, completely suppressing Sn^{2+} oxidation. However, we have to note that the most efficient Pb-free

perovskite solar cells to date are not on par with the performance of Pb containing perovskites.

Table I reports the Pb-free compounds synthesized so far for solar cell applications. Their PCE (in %), open-circuit voltages (in V), and fabrication methods are listed. Among different categories of Pb-free materials, Sn-based ABX_3 type perovskites show the highest PCE. This can be understood by the fact that these Sn-based ABX_3 type perovskite materials exhibit very similar properties to the Pb-based ones, as discussed in Sec. II. It was reported in 2020 for $FASnI_3$ perovskites that partially substituting FA with ethylammonium (EA) and surface passivation with 1,2-diaminoethane (EDA) can promote the crystallinity and energy band alignments with charge transport layers.⁷⁶ As a result, the charge carriers show enhanced mobility and longer lifetimes, resulting in an improved PCE with respect to 9% of the pristine case, with 13.24% and 12.64% for forward and reverse scans, respectively. At the beginning of 2021, the solar cell stability was improved and a maximum efficiency of 13.4% was attained.⁷⁸ The currently certified record efficiency amounts today to 14.6% with negligible hysteresis.⁷⁹ A remarkable photostability improvement was obtained in 2022 from a synergistic chemical engineering approach, leading to over 1300 h operational stability in N_2 with maximum power point (MPP) tracking.⁸⁰ Similarly, the highest reported PCEs of $CsSnI_3$ and $MASnI_3$ until now are 12.96%⁸¹ and 7.78%,⁸² respectively, although it is proven theoretically that their PCEs are limited to 32.3% by comparison to 30.5% for Pb-based solar cells.⁸³ The much lower stability of Sn-based perovskite solar cells by comparison to Pb based ones even when encapsulated, leading to the exploration of surface passivation strategies.⁸⁴ For example, Jøker *et al.*⁸⁵ found that the addition of SnF_2 and $(EDA)I_2$ could improve the PCE and the stability of $FASnI_3$ and that additional 20% doping of nonpolar organic cation, guanidinium (GA^+), could increase the PCE from 7.1% to 8.5%. Furthermore, when the material ages after storage in a glove-box environment for 2000 h, the PCE of the same device tends to be 10%. Devices made of the hybrid perovskite $(GA, FA)SnI_3$ remain stable for 1 h under continuous 1-sun illumination and for 6 days in the dark and in air without encapsulation. Very recently, dipropylammonium iodide (DipI) together with the reducing agent sodium borohydride ($NaBH_4$) was shown to prevent the premature degradation of the Sn-based devices. Efficiencies above 10% were achieved with enhanced stability with 5 h in air [60% relative humidity (RH)] at MPP and 96% of the initial PCE after 1300 h at MPP in the N_2 atmosphere.⁸⁰ According to the reported device I–V characteristics, the highest V_{OC} of Sn based perovskite solar cells reported so far is 0.96 V,⁷⁹ which is still significantly lower than the expected ideal value,⁸³ while the highest V_{OC} of Pb based perovskite solar cells is closer to the physical limit being over 1.3 V.⁸⁶

Ge-based perovskite solar cells have achieved lower efficiencies than Sn-based ones (see Table I). Ge^{2+} oxidation under ambient air conditions causes structure instability, which is similar to the outcome of the Sn^{2+} oxidation in Sn-based perovskites. As an alternative, perovskite solar cells using alloys of Ge and Sn are developed, showing promising PCEs and better stabilities than their pure Ge equivalents due to the native-oxide passivation of surfaces. The energy band structure behavior of Sn/Ge perovskite compounds is completely different from the Sn/Pb alloys that show bandgap bowing.¹⁵⁸ Indeed, their bandgaps ($R3m$ space group) are linearly

TABLE I. Solar cell applications of different Pb-free halide perovskites and their power conversion efficiencies (PCE, in %), open-circuit voltages (V_{OC} , in V), and fabrication methods. Boldface denotes state of the art results.

| Category | Compounds | PCE (%) | V_{OC} (V) | Fabrication method | Reference |
|------------------|---|-------------------------|--------------|---|-----------|
| | | 7.78 | 0.66 | Spin-coating | 82 |
| | | 7.13 | 0.486 | Two-step thin film deposition method | 87 |
| | | 6.4 | 0.88 | Spin-coating | 25 |
| | | 5.44 | 0.716 | Spin-coating | 88 |
| | MASnI ₃ | 5.23 | 0.68 | Spin-coating | 24 |
| | | 3.89 | 0.38 | Spin-coating with SnF ₂ additive and hydrazine vapor treatment | 89 |
| | | 3.15 | 0.46 | Spin-coating with SnF ₂ additive | 90 |
| | | 2.14 | 0.45 | Spin-coating with solvent bathing | 91 |
| | | 1.94 | 0.25 | Spin-coating with SnF ₂ additive | 92 |
| | | 1.86 | 0.273 | Low-temperature vapor assisted solution deposition process | 93 |
| | | 1.7 | 0.38 | Thermal co-evaporation | 93 |
| | MASnI ₂ Br | 5.48 | 0.77 | Spin-coating | 24 |
| | MASnI ₂ Br ₂ | 5.73 | 0.82 | Spin-coating | 24 |
| | MASnBr ₃ | 4.27 | 0.88 | Spin-coating | 24 |
| | | 1.12 | 0.498 | Vapor deposition | 94 |
| | MASnBr _{0.5} I _{2.5} | 1.05 | 0.18 | Spin-coating | 95 |
| | MASnI _{1.8} Cl _{0.2} | 3.1 | 0.38 | Drop casting | 96 |
| | MA _{0.9} CS _{0.1} SnI ₃ | 0.51 | 0.49 | Vapor assisted solution deposition process | 97 |
| | | 0.3 | 0.20 | Spin-coating | 98 |
| | (FA _{0.9} EA _{0.1}) _{0.98} EDA _{0.02} SnI ₃ | 13.2 | 0.84 | Spin-coating with GeI ₂ additive | 76 |
| | FA _{0.98} EDA _{0.01} SnI ₃ | 12.2 | 0.70 | 92 days of storage in N ₂ : 80% PCE | 99 |
| | PEA _{0.15} FA _{0.85} SnI ₃ + NH ₄ SCN | 12.4 | 0.94 | Spin-coating with SnF ₂ additive | 100 |
| | FA _{0.9} EA _{0.1} SnI ₃ | 11.75 | 0.65 | Spin-coating with GeI ₂ additive | 76 |
| | PEA _{0.15} FA _{0.85} SnI ₃ | 7.1 | 0.78 | Spin-coating with SnF ₂ additive | 100 |
| | FASnI ₃ + 4-(aminomethyl) piperidinium | 10.9 | 0.69 | Spin coating | 101 |
| | FASnI ₃ | 10.1 | 0.63 | Spin coating with FAI, SnI ₂ , and SnF ₂ additive | 102 |
| | | 13.4 | 0.81 | Spin-coating with phenylhydrazine | 78 |
| | | 14.6^a | 0.96 | Spin-coating with adducts | 79 |
| | | 10.6 | 0.66 | Stability record^a | 80 |
| | FASnI ₃ | 9.03 | 0.72 | Spin-coating with GeI ₂ additive | 76 |
| | | 6.75 | 0.58 | Spin-coating with Sn powder additive | 103 |
| | | 6.6 | 0.48 | Spin-coating with SnF ₂ additive | 104 |
| | | 6.48 | 0.553 | Spin-coating with SnF ₂ additive | 105 |
| | | 6.22 | 0.48 | Spin-coating with SnF ₂ additive | 106 |
| | | 5.27 | 0.38 | Spin-coating with diethyl ether dripping and SnF ₂ additive | 107 |
| ABX ₃ | | 4.8 | 0.32 | Spin-coating with pyrazine mediator and SnF ₂ additive | 107 |
| | | 3.12 | 0.31 | Spin-coating with SnF ₂ and HPA additive | 108 |
| | | 2.10 | 0.24 | additive Spin-coating | 109 |
| | | 8.92 | 0.63 | Spin-coating with SnF ₂ additive | 105 |
| | FASnI ₃ + 2,3-diaminopropionic acidmonohydrochloride (2,3-DAPAC) | 7.23 | 0.52 | Spin-coating with SnF ₂ additive | 110 |

TABLE I. (Continued.)

| Category | Compounds | PCE (%) | V _{OC} (V) | Fabrication method | Reference |
|----------|--|---------|---------------------|---|-----------|
| | FASnI ₂ Br | 1.72 | 0.47 | Spin-coating | 109 |
| | Br-doped FASnI ₃ | 5.5 | 0.41 | Spin-coating with pyrazine mediator and SnF ₂ additive | 111 |
| | FA _{0.8} MA _{0.2} SnI ₃ | 1.4 | 0.24 | Spin-coating solvent engineering | 98 |
| | FA _{0.25} MA _{0.75} SnI ₃ | 4.49 | 0.48 | Spin-coating with SnF ₂ additive | 104 |
| | FA _{0.5} MA _{0.5} SnI ₃ | 5.92 | 0.53 | Spin-coating with SnF ₂ additive | 104 |
| | FA _{0.75} MA _{0.25} SnI ₃ | 8.12 | 0.61 | Spin-coating with SnF ₂ additive and chlorobenzene dripping | 104 |
| | | 9.06 | 0.55 | Spin-coating + SnF ₂ additive and chlorobenzene dripping + post-annealing | 112 |
| | FA _{0.75} MA _{0.25} SnI ₃ CsSnI ₃ + phthalimide (PTM) | 7.2 | 0.55 | Spin-coating with SnF ₂ additive and hot antisolvent treatment and solvent vapor annealing | 113 |
| | | 3.31 | 0.46 | Spin-coating + antisolvent | 114 |
| | | 2.60 | 0.37 | Spin-coating + SnF ₂ additive | 115 |
| | | 10.1 | 0.64 | Two-step spin-coating + chlorobenzene as antisolvent | 77 |
| | CsSnI ₃ + thiosemicarbazide (TSC) | 8.20 | 0.63 | Passivator assisting sequential vapor deposition | 84 |
| | CsSnI ₃ | 4.81 | 0.38 | Spin-coating with SnI ₂ additive | 116 |
| | | 3.83 | ... | Spin-coating with SnF ₂ and piperazine additive | 117 |
| | | 3.56 | 0.50 | Spin-coating with SnCl ₂ additive | 118 |
| | | 3.31 | 0.52 | Spin-coating and annealing | 119 |
| | | 2.76 | 0.43 | Spin-coating with SnI ₂ additive | 120 |
| | CsSnI ₃ | 2.02 | 0.24 | Spin-coating with SnF ₂ additive | 121 |
| | FA _{0.75} MA _{0.25} Sn _{0.95} Ge _{0.05} I ₃ | 1.83 | 0.17 | Spin-coating with SnF ₂ additive and hydrazine vapor treatment | 89 |
| | | 1.70 | ... | Solid-state reaction | 32 |
| | | 1.66 | 0.20 | Spin-coating with SnF ₂ additive | 81 |
| | | 0.90 | 0.42 | Sequential evaporation and subsequent annealing | 121 |
| | | 7.90 | 0.45 | Spin-coating + GeI ₂ and SnF ₂ additives | 115 |
| | FA _{0.75} MA _{0.25} Sn _{0.95} Ge _{0.05} I ₃ Native oxide passivated | 4.48 | 0.42 | Spin-coating + antisolvent | 114 |
| | | 7.11 | 0.63 | Solid-state reaction | 32 |
| | CsSn _{0.5} Ge _{0.5} I ₃ | 3.72 | 0.48 | Solid-state reaction + N ₂ | 32 |
| | CsSn _{0.5} Ge _{0.5} I ₃ | 1.76 | 0.22 | Spin-coating with SnF ₂ additive | 122 |
| | CsSnI _{2.9} Br _{0.1} | 1.67 | 0.29 | Spin-coating with SnF ₂ additive | 81 |
| | CsSnI ₂ Br | 3.20 | 0.31 | Sequential evaporation and subsequent annealing | 122 |
| | CsSnI ₂ Br | 1.56 | 0.31 | Sequential evaporation and subsequent annealing | 81 |
| | CsSnBr ₃ | 3.04 | 0.37 | Spin-coating with SnF ₂ additive and hydrazine vapor treatment | 89 |
| | | 2.10 | 0.41 | Spin-coating with SnF ₂ additive | 123 |
| | CsSnBr ₃ | 0.95 | 0.41 | Spin-coating with SnF ₂ additive | 81 |
| | CsSnI ₃ (QR) | 0.55 | 0.45 | All vapor deposited with SnF ₂ additive | 124 |
| | | 13.0 | 0.86 | Spin-coating | 81 |
| | CsSnBr ₃ (QR) | 10.5 | 0.85 | Spin-coating | 81 |
| | CsSnCl ₃ (QR) | 9.66 | 0.87 | Spin-coating | 118 |

TABLE I. (Continued.)

| Category | Compounds | PCE (%) | V _{OC} (V) | Fabrication method | Reference |
|--|--|-------------------------|---------------------|--|-----------|
| | MAGeI ₃ | 0.68 | ... | ... | 125 |
| | MAGeI ₃ | 0.20 | 0.150 | ... | 125 |
| | MAGeI _{2.7} Br _{0.3} | 0.57 | 0.449 | Spin-coating | 125 |
| | CsGeX ₃ | 4.94 | 0.51 | Quantum rods | 126 |
| | CsGeI ₃ | 0.11 | 0.074 | ... | 127 |
| | {en}MASnI ₃ | 6.63 | 0.43 | Spin-coating with SnF ₂ additive | 128 |
| | {en}FASnI ₃ | 7.14 | 0.48 | Spin-coating with SnF ₂ additive | 29 |
| | {en}FA _{0.78} GA _{0.22} SnI ₃ | 9.60 | 0.619 | Spin-coating with SnF ₂ additive | 85 |
| | Cs ₂ AgBiBr ₆ + carboxy-chlorophyll derivative (C-chl) | 3.11^a | 1.04 | Spin-coating | 129 |
| | Cs ₂ AgBiBr ₆ | 2.84 | 1.06 | Spin-coating | 130 |
| | Cs ₂ AgBiBr ₆ | 2.43 | 0.98 | Spin-coating | 131 |
| A ₂ BB'X ₆ | (Cs _{0.9} Rb _{0.1}) ₂ AgBiBr ₆ | 2.23 | 1.01 | Spin-coating with antisolvent | 132 |
| | | 1.44 | 1.04 | Spin-coating | 132 |
| | | 1.26 | 1.02 | Spin-coating with antisolvent | 131 |
| | | 1.37 | 1.12 | Sequential vapor deposition | 133 |
| | Cs ₂ NaBiI ₆ | 1.52 | 0.99 | Spin-coating | 134 |
| | Cs ₂ NaBiI ₆ | 0.42 | 0.47 | One-step hydrothermal process | 135 |
| | Cs ₂ SnI ₆ | 0.96 | 0.51 | Thermal evaporation, annealing, and phase change | 136 |
| | Cs ₂ SnI ₆ | 0.86 | 0.52 | Spin-coating | 137 |
| | Cs ₂ SnI ₅ Br | 1.47 | 0.37 | Two-step thin film deposition method | 138 |
| | | 0.47 | 0.25 | Chemical bath deposition | 139 |
| | Cs ₂ SnI ₄ Br ₂ | 1.60 | 0.44 | Two-step thin film deposition method | 138 |
| A ₂ BX ₆ | Cs ₂ SnI ₄ Br ₂ | 2.03 | 0.56 | Two-step thin film deposition method | 138 |
| | Cs ₂ SnI ₂ Br ₄ | 1.08 | 0.58 | Two-step thin film deposition method | 138 |
| | Cs ₂ SnIBr ₅ | 0.002 | 0.57 | Two-step thin film deposition method | 138 |
| | Cs ₂ TiBr ₆ | 3.28 | 1.02 | Two-step vapor deposition | 140 |
| | Cs ₂ TiBr ₆ | 2.26 | 0.89 | Two-step vapor deposition | 140 |
| | Cs ₂ SnI ₃ Br ₃ | 3.63^a | 0.70 | Two-step thin film deposition method with Z907 dye | 141 |
| | | 1.64 | 0.81 | Deposition and homogeneous transformation | 63 |
| | | 0.42 | 0.67 | Deposition and homogeneous transformation | 142 |
| | | 0.39 | 0.81 | Thermal evaporation, spin-coating, and annealing | 143 |
| | | 0.36 | 0.65 | Solvent engineering | 144 |
| | MA ₃ Bi ₂ I ₉ | 0.31 | 0.51 | Spin coating | 145 |
| | MA ₃ Bi ₂ I ₉ | 0.26 | 0.56 | Spin-coating | 63 |
| | MA ₃ Bi ₂ I ₉ Cl _x | 0.19 | 0.35 | Spin-coating | 146 |
| | | 0.12 | 0.68 | Spin-coating | 146 |
| | | 0.11 | 0.72 | Solvent engineering | 147 |
| | | 0.08 | 0.69 | Spin coating with gas-assisted | 148 |
| | | 0.07 | 0.66 | Spin coating | 149 |
| | | 0.053 | 0.84 | Spin-coating | 150 |
| | MA ₃ Sb ₂ I ₉ | 0.003 | 0.04 | Spin-coating | 146 |
| | | 2.77 | 0.70 | Spin-coating with pyrene/HI + chlorobenzene additive | 151 |
| | MA ₃ Sb ₂ I ₉ | 2.46 | 0.69 | Spin-coating with perylene/HI + chlorobenzene additive | 151 |
| A ₃ B ₂ X ₉ | MA ₃ Sb ₂ I ₉ | 2.25 | 0.63 | Spin-coating with HI + chlorobenzene additive | 151 |
| | MA ₃ (Sb _{0.6} Sn _{0.4}) ₂ I ₉ | 1.89 | 0.62 | Spin-coating with HI additive | 151 |
| | | 2.04 | 0.62 | Spin-coating with HI additive | 152 |
| | | 0.62 | 0.75 | Spin-coating with chlorobenzene dripping | 153 |
| | | 0.5 | 0.89 | Spin-coating | 154 |
| | CsBi ₃ I ₁₀ | 2.80^a | 0.57 | Spin-coating with chlorobenzene dripping | 153 |

TABLE I. (Continued.)

| Category | Compounds | PCE (%) | V _{OC} (V) | Fabrication method | Reference |
|----------|--|---------|---------------------|---------------------------------------|-----------|
| | CsBi ₃ I ₁₀ | 0.40 | 0.31 | Spin-coating | 155 |
| | Cs ₃ Bi ₂ I ₉ | 1.09 | 0.85 | Spin-coating | 146 |
| | Cs ₃ Bi ₂ I ₉ | 0.02 | 0.26 | Spin-coating | 155 |
| | Cs ₃ Sb ₂ I ₉ | 0.84 | 0.60 | Spin-coating with HI additive | 152 |
| | Rb ₃ Sb ₂ I ₉ | | | | |
| | Cs ₃ Sb ₂ I ₉ | <1 | 0.30 | Dual annealing | 152 |
| | Rb ₃ Sb ₂ I ₉ | | | | |
| | (NH ₄) ₃ Sb ₂ I ₉ | 0.66 | 0.55 | Spin-coating with toluene dripping | 156 |
| | (NH ₄) ₃ Sb ₂ I ₉ | 0.51 | 1.03 | Spin-coating with chloroform dripping | 157 |

^aThe highest value of PCE for each category of Pb-free perovskites, as highlighted in a bold font.

increasing with respect to the concentration of Ge.¹⁵⁹ For instance, the CsSn_{0.5}Ge_{0.5}I₃ has a bandgap (1.50 eV) in between CsSnI₃ (1.31 eV) and CsGeI₃ (1.63 eV) and allows photo-absorption across the visible light region.³² As a result, a PCE of 7.11% is obtained for CsSn_{0.5}Ge_{0.5}I₃ in comparison to the 3.72% attained without forming a native-oxide layer and the 1.7% of the pure CsSnI₃. As discussed previously, mixing halides might lead to chemical inhomogeneities in the conventional perovskite compounds. However, mixed-halide CsSn_{1-x}Ge_xI_{3-y}Br_y compounds are easier to synthesize than the single-halide CsSn_{1-x}Ge_xI₃ compounds and are superior in terms of optical response in the visible light range, according to Chang *et al.*¹⁶⁰ Among them, the CsSn_{0.5}Ge_{0.5}I₂Br is the best choice. To date, the highest PCE of Sn/Ge alloys amounts to 7.9%, with FA_{0.75}MA_{0.25}Sn_{0.95}Ge_{0.05}I₃ based solar cells fabricated by passivating and reducing trap densities with GeI₂ and SnF₂ additives.¹¹⁵ More importantly, the PCE retains 91% of its initial value for 500 h under 1-sun illumination in air. Although the results of Sn/Ge mixed perovskites are encouraging, they are still far from the expected maximum PCE value. For instance, the theoretical predicted PCE of CsSn_{0.5}Ge_{0.5}I₃ is as high as 24.20%.¹⁶¹

Double perovskites and vacancy ordered double perovskites are very stable under ambient conditions. Yet, the electronic bandgaps of the synthesized double perovskites range from 2 to 3.4 eV and thus are too large for efficient light harvesting in single-junction photovoltaics. The highest PCE obtained for a double perovskite, 3.11% obtained for Cs₂AgBiBr₆, is, nevertheless, a decent achievement for a large bandgap semiconductor.¹²⁹ Doping with In, a common strategy for highly efficient light emitters discussed below, could also improve the attained photovoltaic performance as recently shown by Schade *et al.*¹⁶² More generally, their stability combined with their optoelectronic properties, including photoconversion at high energy, light emission, and charge transport, might be more attractive for other optoelectronic applications.

Meanwhile, the highest PCE obtained for a vacancy ordered double perovskite is 3.63% for the mixed-halide Cs₂SnI₃Br₃.¹⁴¹ Since the Sn atoms used in vacancy ordered double perovskites correspond to the +4 oxidation state, these perovskite structures are the most stable among Sn based perovskite materials under ambient conditions.

Although Pb-free A₃B₂X₉ 2D perovskite derivatives are quite stable in air, their achieved PCE remained much lower than 1% without improvement for a long time. A breakthrough was obtained in 2018 for Pb-free 2D perovskite based on Sb dimers with the help of additives and antisolvents treatment. A continuum, smooth, and pinhole-free morphology of MA₃Sb₂I₉ can be formed, thanks to fast heterogeneous nucleation, yielding a record PCE of 2.77%.¹⁵¹ In the same year, a PCE of 2.80% was achieved for MA₃(Sb_{1-x}Sn_x)₂I₉ by heterovalent substitution when x is 0.4, contrasting to a PCE of 0.62% when x is 0.¹⁵³ By Sn⁴⁺ substitution, the bandgap is reduced from the pristine bandgap value of 2 eV close to the optimum value of 1.55 eV, and the electronic conductivity is changed from p-type to n-type, leading to a better band alignment with the selected contact layers. All the above discussions point out that chemical engineering, additives, antisolvent treatment, and hydrophobic charge transport layers are the guides to further improve the PCEs of double and 2D Pb-free perovskites.

To establish a connection between the types of Pb-free materials and their application in solar cells, we calculate the percentage of each type of Pb-free materials that have been reported in solar cell applications. Figure 2(a) highlights the contribution of the conventional single ABX₃ (pink color), double A₂BB'X₆ (cyan color), vacancy ordered double A₂BX₆ (gray color), and 2D layered A₃B₂X₉ Pb-free perovskites (orange color) by the inner ring of the sunburst chart, where their percentages are listed at the inner blank spaces, which are 62%, 7%, 9%, and 22%, respectively. In addition, the contributions of different types of B site cations are highlighted by the outer ring of the sunburst chart, where the corresponding percentages are summarized at the outer blank spaces. In addition, the contribution of A site cations and X site anions is represented by the 3D pie charts, where their corresponding percentages are summarized next to each of them.

Among all Pb-free compounds, most materials contain Sn, with 90% of the cubic perovskites and 82% of the vacancy ordered double perovskites being Sn-based compounds. This is in line with the favorable PCEs of Sn based perovskite solar cells being the most promising to date. Among all Sn-based compounds used for solar cell applications, 89% of Sn compounds are materials with Sn in the +2 oxidation state, which is consistent with the fact that stability

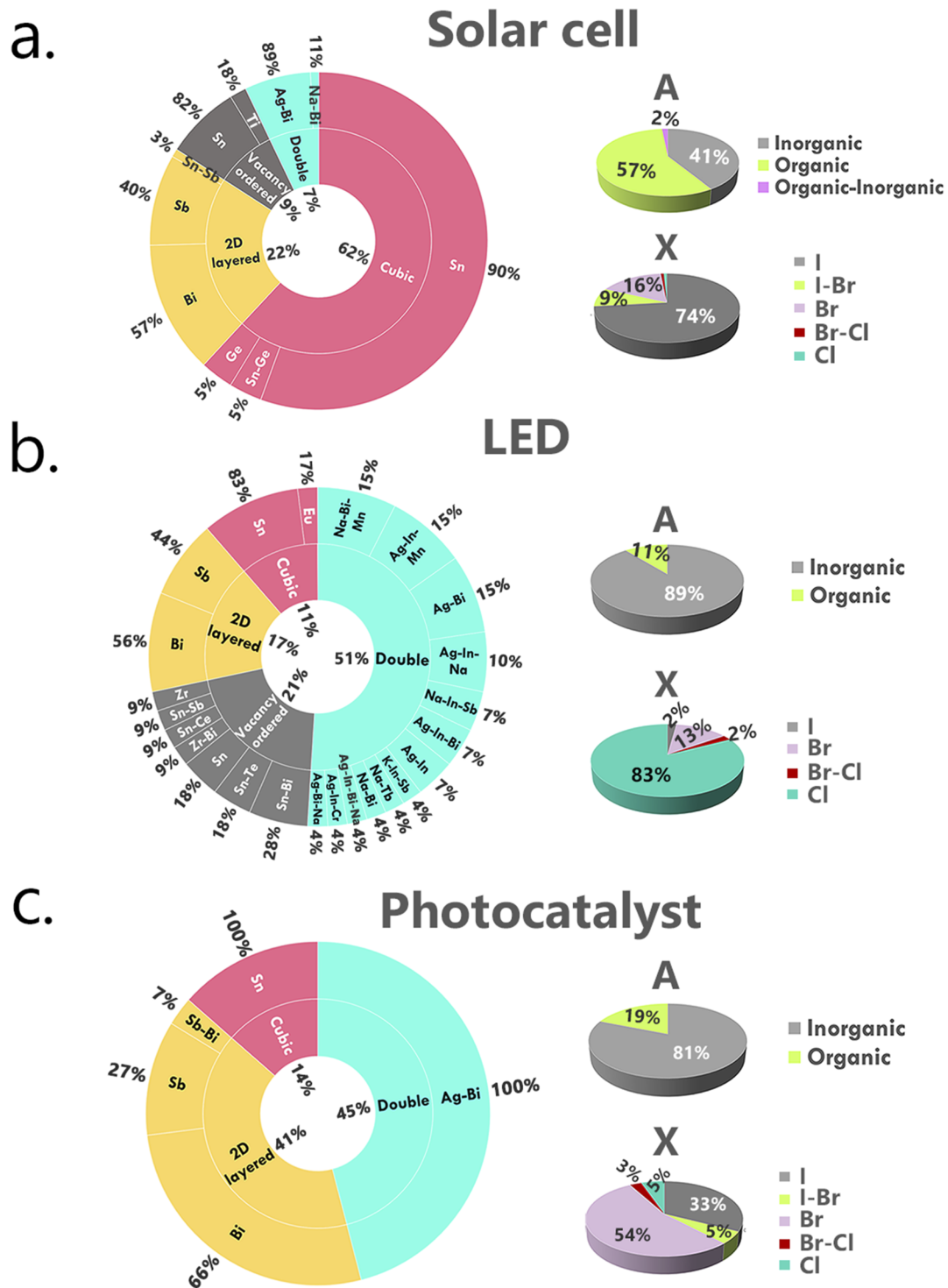


FIG. 2. Sunburst charts showing the use of different Pb-free halide perovskite classes (conventional ABX_3 in pink, double $A_2BB'X_6$ in cyan, vacancy ordered double A_2BX_6 in gray, and 2D layered $A_3B_2X_9$ in orange) in the fabrication of solar cells (top), LEDs (middle), and photocatalysts (bottom). In each chart, the contribution of different perovskite classes is highlighted by the inner ring, and their percentages are summarized at the inner blank spaces; the contribution of different B site cations in each class is highlighted by the outer ring with the same color as the inner ring, and their percentages are summarized at the outer blank spaces. The corresponding distribution in terms of different A site cations and X site anions is shown in the 3D pie charts (right panels). Percentages below 1% are not included.

remains the main issue in this field. Therefore, the still rare (5%) use of either pure Ge (5%) or mixtures of Ge and Sn might become the next step in the quest for stable Pb-free perovskite solar cell applications. Among $A_2BB'X_6$ double perovskites, the ones based on $B = \text{Bi}$ and $B' = \text{Ag}$ (including doped derivatives) are almost the sole Pb-free candidates to date that have been tested for solar cells; those based on $B = \text{Bi}$ and $B' = \text{Na}$ have merely achieved a PCE of 0.4%. In addition, in 2D layered perovskites, most of the B site cations are either Bi (57%) or Sb (40%), with a small percentage (3%) of Bi–Sb mixtures. In addition, from the 3D pie chart indicative of the halide species, as for Pb-based perovskites, most compositions used for solar cell applications are iodides (74%), followed by bromides (16%) and mixed I–Br compounds (9%). In contrast, the Cl and mixed Br–Cl compounds are rarely used (less than 1%). Finally, organic (57%) and inorganic (41%) A-site cations are almost equally used, with a small amount (2%) of organic–inorganic mixtures.

IV. LIGHT EMISSION

Over the past decades, thanks to their intrinsic properties, including high PLQY, Pb-based metal halide perovskites have also gained great interest for LED applications. For example, Zhou *et al.*¹⁶³ achieved a record-high PLQY of 94.6% with MAPbX_3 ($X = \text{Cl}, \text{Br}, \text{I}$) nanocrystals embedded in polyvinylidene fluoride composite films. However, achieving large external quantum efficiencies (EQE) in operating LED devices requires more, especially good carrier transport and carrier injection from the electrical contacts toward the active zone. Once these conditions are fulfilled, it is considered nowadays that perovskite-based LEDs should overcome EQE of 20% starting from high PLQY, thanks to photon recycling and efficient optical outcoupling.¹⁶⁴ Green LEDs are the best performing devices, leading to a maximum EQE of 28.1% in 2021.¹⁶⁵ Using non-perovskite matrices was also successful for Pb-based green emitters leading to stable operation over 50 h with an EQE of 15%.¹⁶⁶ This solution has the disadvantage of putting strong practical limits on the current injected into the active zone (1.2 mA cm⁻² in Ref. 166) but may provide some guidance for the design of Pb-free emitters. Pb-based red LEDs emitting at 627 nm with an impressive EQE of 20.3% (starting from a PLQY of 88%) were obtained recently, although the operational stability remains limited to 1 h and the EQE drops very quickly for current densities above 1 mA cm⁻². The performances of blue Pb-based LEDs are more limited leading, for example, to an EQE of 12.3% starting from a PLQY over 90%,¹⁶⁷ or a sky-blue emitting device with an EQE of 13.8% but driven by a high voltage of above 4 V.¹⁶⁸ Finally, it shall be mentioned that demonstrations of single layer Pb-based white light LED do exist,¹⁶⁹ although with room for improvement. A promising EQE of 1.2% (starting from a PLQY of 85%) with a color rendering index (CRI) of 93 was, for example, obtained in 2020 using CsPbCl_3 quantum dots doped with Sm^{3+} .¹⁷⁰ It is now clear that Pb-based perovskites are nowadays strong competitors in the field of LEDs, with remarkable EQE demonstrations for monochromatic red, green, or blue optical sources and even promising single layer white-light emitters. However, challenges are still remaining for commercialization including among others, highly efficient blue electroluminescence, long device lifetime, toxicity, and bioavailability of lead.¹⁷¹

From the perspective of LED engineering, the quality of the interfaces is of utmost importance as mentioned above. This additional constraint might hinder the practical application of most Pb-free perovskite materials to LEDs, despite exhibiting attractive PLQY. So far, most of the experimental data reported on Pb-free materials to illustrate light emission capabilities are related to the PLQY. This interesting piece of information shall be handled with care since it might not guarantee LEDs with attractive performances. We already saw indeed in Sec. III on solar cells that interface issues are limiting the performances of Pb-free perovskite devices. It shall be further pointed out that current densities flowing through operating LED devices may exceed by one order of magnitude the current densities observed in solar cells. This may put even more stringent requirements on the Pb-free material quality and their interfaces with carrier transporting layers. In this Perspective, we, nevertheless, limit our overview of Pb-free perovskite performances to PLQYs, leaving aside EQEs mainly due to the lack of extensive data in the literature.

As it seems Pb-free materials can hardly compete with Pb-based ones for solar cells due to their low PCEs, this might be also the case for LED applications. Their high tunability across the entire visible light spectrum might be nevertheless one comparative advantage.^{163,172–174} Narrowband emission, usually observed at low temperature, is very often attributed to intrinsic free excitonic transitions. Such transitions can be influenced by lattice parameters and thermal expansion mismatches between perovskites and charge transport layers. An additional broadband emission at low energy is also observed in some cases. This broadband emission is believed to have good potential for white light LEDs. Self-trapping excitons (STEs) are very often claimed to be at the origin of this broad red-shifted, but extrinsic or defect-related emission mechanisms are still not ruled out.

Among the four classes of Pb-free perovskites, double perovskites and vacancy ordered double perovskites show promising PLQYs as well as high intrinsic thermodynamic stabilities and low carrier effective masses. One of the major challenges is their wide and/or indirect bandgaps, which makes them less suitable for optoelectronic applications in the visible region. For this reason, homovalent and heterovalent co-doping have been developed. $\text{Cs}_2\text{AgBiCl}_6$ and $\text{Cs}_2\text{AgInCl}_6$ have become the reference materials for realizing white light LEDs for Pb-free materials. In comparison to pure $\text{Cs}_2\text{AgBiCl}_6$, the higher stability of Na-doped $\text{Cs}_2(\text{Na}_{1-x}\text{Ag}_x)\text{BiCl}_6$ was attributed to the easier formation of a $[\text{NaCl}_6]^{5-}$ octahedron compared to a $[\text{AgCl}_6]^{5-}$ one, but this, in turn, results in a larger bandgap.¹⁷⁵ It is also found that the minor luminescence of the as-prepared $\text{Cs}_2\text{NaInCl}_6$ nanocrystals (dark STEs) can convert into a bright yellow emission (attributed to bright STEs) by Ag^+ doping.¹⁷⁶ Two physical mechanisms have been proposed to explain the enhanced light emissions.¹⁷⁷ First, $[\text{NaCl}_6]^{5-}$ and $[\text{AgCl}_6]^{5-}$ octahedra can break the parity-forbidden selection rule for the direct optical transition hence stimulating effective photoluminescence (PL) emission. Second, the presence of Ag^+ can mitigate the effect of lattice vibrations on PL quenching. Sb^{3+} , In^{3+} , and Mn^{2+} doping are also popular choices for tuning the electronic properties. For example, the Sb- and In-doping of $\text{Cs}_2\text{AgBiBr}_6$ induce opposite variations of the bandgaps, leading to an increase (decrease) for In^{3+} (Sb^{3+}) doping. It has to be noted that Sb^{3+} doping produces the smallest bandgap within this class, with a value of

1.86 eV for $\text{Cs}_2\text{Ag}(\text{Bi}_{0.625}\text{Sb}_{0.375})\text{Br}_6$. In addition, these doped systems are only stable when In^{3+} and Sb^{3+} doping ratios are within the 0%–75% and 0%–37.5% ranges, respectively.¹⁷⁸

Substituting or doping double perovskites that contain Bi (or Sb) with In results in an interplay between direct and indirect bandgaps,^{32,155,179} which could be promising for the luminescence of perovskite phosphors toward white-light emission. In contrast, the bandgaps of $\text{Cs}_2\text{AgInCl}_6$ double perovskites have no significant difference before and after Mn^{2+} doping.¹⁸⁰ However, with Mn-doping as high as 1.5%, the weak PL of undoped $\text{Cs}_2\text{NaBiCl}_6$ has been enhanced to emit a new orange-red PL (from 525 to 700 nm). The PLQY increases by an order of magnitude, namely, from 1.6% up to 16%. This enhanced emission has been attributed to the near-UV light absorption of $[\text{BiCl}_6]^{3-}$ octahedra in the host lattice and the energy transfer from Bi^{3+} to Mn^{2+} activators via the spin-forbidden $^4\text{T}_1 \rightarrow ^6\text{A}_1$ transition.¹⁸¹ This $^4\text{T}_1 \rightarrow ^6\text{A}_1$ $d-d$ transition is expected to interact less with nonradiative trap states in the host lattice, accounting for the enhanced PL intensity and millisecond long lifetime.¹⁵⁴ As reported in the literature,¹⁸² the internal quantum efficiency of $\text{Cs}_2(\text{Ag}_{0.4}\text{Na}_{0.6})\text{InCl}_6$: 1% Bi phosphor can be further increased from 89.9% to 98.4% and 98.6% by co-doping 1% Ni and 1% Ce, respectively. The physical mechanisms at the origin of light emission depend on the nature of the perovskite host. Specifically, for Mn-doped $\text{Cs}_2(\text{Na}_{0.75}\text{Ag}_{0.25})\text{BiCl}_6$, the distinct energy-transfer channel from Mn^{2+} ion guest to STEs perovskite host has been proposed to result in the dominant Mn^{2+} emission,¹⁷⁵ which is similar to pure $\text{Cs}_2\text{AgInCl}_6$.¹⁸⁰ In contrast, for Mn-doped $\text{Cs}_2(\text{Na}_{0.4}\text{Ag}_{0.6})\text{In}_{0.95}\text{Bi}_{0.05}\text{Cl}_6$, the efficient energy transfer from broadband STEs host to Mn^{2+} guest $d-d$ transitions would explain the high PLQY.¹⁸³ In addition to the above two mechanisms, for the Mn-doped $(\text{C}_6\text{H}_{18}\text{N}_2\text{O}_2)\text{PbBr}_4$, the tentative explanation for the ultrabroad band warm light emission relies on a simultaneous enhancement of STE emission and Mn^{2+} emission.¹⁸⁴

Table II presents, for the four material classes, the Pb-free perovskite compositions synthesized to date for LED applications, together with their emission peak positions (in nm), the light emission colors, the full-width half maxima (FWHM, in nm) of the emissions, and the PLQYs (in %). We note that the highest PLQY of about 93% has been achieved with Sb-doped $\text{Cs}_2\text{KInCl}_6$.¹⁸⁵ Apart from double perovskites, vacancy ordered double perovskites also appear as promising candidates for LED applications. The highest PLQY among them is obtained for Te-doped Cs_2SnCl_6 , with 95.4%.¹⁸⁶ Replacing Sn^{4+} with Te^{4+} is proposed to lead to the generation of new defect levels above band edges, which promote an exciton transition nearby $[\text{TeCl}_6]^{2-}$ octahedra, thereby initiating STEs emission of broad yellow–green luminescence.¹⁸⁶ This Te^{3+} triggered STEs emission is also hypothesized in the A site organic perovskite $(\text{NH}_4)_2\text{SnCl}_6$, whose PLQY increases from less than 0.05% before Te^{3+} doping to 83.5% after doping.¹⁸⁷ Noteworthy, the good stability against water of the Te-doped Cs_2SnCl_6 makes it particularly suitable for underwater lighting applications.¹⁸⁶

The statistical overview of different classes and compositions of Pb-free perovskites explored to date for LED applications is also shown in Fig. 2(b). Among all Pb-free compounds synthesized for LED applications, 51% are double perovskites and 21% belong to the vacancy ordered double perovskites. The percentages of conventional perovskites and 2D layered perovskites are relatively smaller,

with 11% and 17%, respectively. Unlike in conventional perovskites where the B site is always Sn, in double perovskites, B site cations are often mixtures of two or three types of cations, such as Ag–Bi (15%), Na–Bi–Mn (15%), and Ag–In–Mn (15%). In the 2D layered category, only pure Bi-based or pure Sb-based compositions have been reported, with almost an equivalent proportion. Regarding halides, it appears that Cl (83%) and Br (13%) based materials have widely been explored in the context of LED applications, whereas alloys or iodine compositions are rarer. This is quite different from solar cell applications where the iodides are dominant (74%) due to their lower bandgaps capable to harvest low-energy photons. Finally, inorganic cations are by far the most frequent choice for the A site (89%) in LED applications because of their comparatively higher PLQYs, better stability against heating, and slightly lower hygroscopicity. In addition, no organic–inorganic mixtures for the A site are reported so far.

V. PHOTO-CATALYSIS

The main requirements for a promising photocatalytic material are suitable band alignments and bandgaps, strong light absorption, high chemical stability, efficient charge carrier transport, and good operation in strong acidity and/or alkali environments.^{211–213} Over the past few years, the potential of Pb-based halide perovskites has been investigated as a catalyst for photocatalytic hydrogen (H_2) evolution, CO_2 reduction reaction, and various organic synthesis or chemical reactions.^{212,214}

The performance of a complete water splitting system can be evaluated by introducing the solar-to-hydrogen (STH) conversion efficiency.²¹⁵ STH has reached nowadays values of 19% close to the theoretical limits (30% under light concentration),^{216–218} but progress is needed to significantly lower the cost of the systems and enhance their operational stability.²¹⁹ Naturally, halide perovskites appear as low-cost alternative electrical power sources needed for water splitting, thanks to their excellent photovoltaic performances, but single-junction cells made of efficient perovskite materials for photovoltaic (PV) do not usually produce enough voltage to drive simultaneously the hydrogen evolution reaction (HER) or oxygen evolution reaction (OER) in photocatalytic water splitting. This is not the case for perovskite in tandem solar cell configurations with silicon that exhibit nice STH values up to 18.7% but rely on classical electrode materials.²²⁰ On the other hand, Pb-free perovskite solar cells are still far from reaching the efficiency and operational stability under the ambient condition of their Pb-based counterparts and are thus not the best candidates so far as electrical power sources to be included in complete water splitting systems.

Interestingly, perovskite materials can also directly participate in the chemical reactions at the electrodes. This was first shown in 2016 when MAPbI_3 showed promising performance for photocatalytic water splitting.²²¹ The H_2 evolution rate was measured at $57 \mu\text{mol g}^{-1} \text{h}^{-1}$ with a splitting efficiency of 0.81%. MAPbI_3 is stable at a specific saturation solution where $[\text{I}^-] \leq [\text{H}^+]$ and $\text{pH} \leq -0.5$. In 2018, Wang *et al.*^{222,223} proposed a heterostructure of $\text{MAPbI}_3/\text{TiO}_2/\text{Pt}$ and $\text{MAPbI}_3/\text{Ta}_2\text{O}_5/\text{Pt}$ with significant enhancement in the H_2 evolution rate of 89-fold and 52-fold over MAPbI_3/Pt . From that perspective, Pb-free perovskites may play a more interesting role since the constraint of being an efficient photovoltaic material no longer applies.

TABLE II. Overview of various Pb-free halide perovskites used for LED applications. The emission peak positions (in nm), light emission colors, full-width half maxima (FWHM, in nm) of the emissions, and PLQYs (in %) are indicated. Films, powder, nanocrystals (NCs), or more rarely nanoplatelets or nanocages are used. Boldface denotes state of the art results.

| Category | Compounds | Emission peak (nm) | Color | FWHM (nm) | PLQY (%) | Comment | Reference |
|---|--|--|---------------|-----------|-------------------------|---------------|-----------|
| ABX ₃ | MASn(Br/I) ₃ | 667–945 | ... | ... | <5.3 | Films | 188 |
| | CsSn(Br/I) ₃ | 667–887 | ... | ... | | Films | 54 |
| | CsSnBr ₃ | 670 | Dark red | 56 | 2.1 | Nanocages | 189 |
| | CsSnBr ₃ | 672 | Red | 54 | 9.1 | Films | 190 |
| | CsSnI ₃ | 950 | Infrared | | 3.8 | Films | 191 |
| | CsBr: Eu ²⁺ | 440 | White | 31 | 32.8^b | NCs | 192 |
| A ₂ BB'X ₆ | Cs ₂ AgBiCl ₆ | 395 | ... | 68 | 6.7 | NCs | 193 |
| | | 610 | ... | 200 | 3 | Powder | 175 |
| | Cs ₂ AgBiBr ₆ | 465 | ... | 82 | 0.7 | NCs | 193 |
| | Cs ₂ (Na _{0.75} Ag _{0.25})BiCl ₆ | 610 | ... | 160 | 45 | Powder | 175 |
| | Cs ₂ (Na _{0.4} Ag _{0.6})InCl ₆ : Bi ³⁺ | 552 | White | 40.9 | 86.2 | Powder | 177 |
| | Cs ₂ (Na _{0.4} Ag _{0.6})InCl ₆ : 5.49% Ho ³⁺ | 490 | White | | 60.5 | Powder | 194 |
| | Cs ₂ Ag(In _{0.875} Bi _{0.125})Cl ₆ | 585 | White | ... | 70.3 | Powder | 195 |
| | Cs ₂ NaBiCl ₆ | 730 | ... | ... | | Powder | 181 |
| | Cs ₂ NaBiCl ₆ : Mn ²⁺ | 590 | | | 15 | Powder | 181 |
| | Cs ₂ Na _{0.995} Bi _{0.995} Mn _{0.01} Cl ₆ | 590 | Orange–red | ... | 11.4 | Powder | 181 |
| | Cs ₂ Na _{0.987} Bi _{0.987} Mn _{0.026} Cl ₆ | 590 | Orange–red | ... | 12.4 | Powder | 181 |
| | Cs ₂ Na _{0.969} Bi _{0.969} Mn _{0.062} Cl ₆ | 590 | Orange–red | ... | 15.1 | Powder | 181 |
| | Cs ₂ AgInCl ₆ | 560 | White | ... | 1.6 | NCs | 180 |
| | | ... | ... | ... | 6 | NCs | 196 |
| | Cs ₂ AgBi _{0.085} In _{0.915} Cl ₆ | 600 | White | 200 | 34 | Powder | 197 |
| | Cs ₂ AgIn _{0.9} Cr _{0.1} Cl ₆ | 1010 | Near-infrared | 180 | 23.5 | Powder | 198 |
| | Cs ₂ NaInCl ₆ : 10% Ag | 535 | Yellow | ... | 31.1 | NCs | 176 |
| | Cs ₂ Ag _{0.4} Na _{0.6} InCl ₆ | ... | ... | ... | 22 | NCs | 196 |
| | Cs ₂ AgInCl ₆ : 0.9% Mn ²⁺ | 632 | White | ... | 3–5 | Powder | 199 |
| | Cs ₂ AgInCl ₆ : 0.5% Mn ²⁺ | 620 | Orange | ... | 9 | NCs | 180 |
| | Cs ₂ AgInCl ₆ : 1.5% Mn ²⁺ | 620 | Orange | ... | 16 | NCs | 180 |
| | Cs ₂ AgInCl ₆ : Mn ²⁺ | 630 | ... | ... | 2 | Powder | 181 |
| | Cs ₂ NaInCl ₆ : 1% Sb ³⁺ | 445 | Blue | | 82 | Powder | 185 |
| | Cs ₂ KInCl ₆ : 5% Sb ³⁺ | 495 | Green | | 93^a | Powder | 185 |
| | Cs ₂ NaEuCl ₆ | 593 | Red | ... | 35 | Powder | 200 |
| | Cs ₂ NaTbCl ₆ | 548 | Green | ... | 56 | Powder | 200 |
| | A ₂ BX ₆ | Cs ₂ SnCl ₆ : 2.75% Bi ³⁺ | 455 | White | 66 | 78.9 | Powder |
| Cs ₂ SnCl ₆ : 1.16% Bi ³⁺ | | 457 | White | 63 | 68.3 | Powder | 201 |
| Cs ₂ SnCl ₆ : 0.11% Bi ³⁺ | | 454 | White | 65 | 67.6 | Powder | 201 |
| Cs ₂ SnCl ₆ : Sb ³⁺ | | 602 | White | 101 | 37 | Powder | 202 |
| Cs ₂ SnCl ₆ : Ce ³⁺ | | 455 | | 80 | 6.57 | NCs | 203 |
| Cs ₂ SnCl ₆ : Te ³⁺ | | 580 | Yellow–green | <100 | 95.4^d | Powder | 186 |
| (NH ₄) ₂ SnCl ₆ : 0.5% Te ³⁺ | | 590 | Orange | 127 | 83.5 | Powder | 187 |
| Cs ₂ SnI ₆ | | 643–742 | ... | 75 | 28 | Nanoplatelets | 204 |
| (NH ₄) ₂ SnCl ₆ | | 590 | ... | 127 | <0.05 | Powder | 187 |
| Cs ₂ ZrCl ₆ | | ... | ... | ... | 31 | Powder | 205 |
| Cs ₂ ZrCl ₆ : Bi ³⁺ | | 456 | Blue | 63 | 50 | Powder | 205 |

TABLE II. (Continued.)

| Category | Compounds | Emission peak (nm) | Color | FWHM (nm) | PLQY (%) | Comment | Reference |
|---|---|--------------------|--------|-------------------------|----------|---------|-----------|
| A ₃ B ₂ X ₉ | Cs ₃ Bi ₂ Br ₉ | 410 | Blue | 48 | 19.4 | NCs | 206 |
| | Cs ₃ Bi ₂ Cl ₉ | 393 | Blue | 59 | 26.4 | NCs | 206 |
| | Cs ₃ Sb ₂ Br ₉ | 410 | Blue | 41 | 46 | NCs | 63 |
| | Cs ₃ Sb ₂ Cl ₉ | 370 | ... | 52 | 11 | NCs | 63 |
| | Cs ₃ Sb ₂ I ₉ | 560 | ... | 56 | 23 | NCs | 63 |
| | Cs ₃ Sb ₂ Br ₉ | 408 | Violet | ... | 51.2 | NCs | 207 |
| | FA ₃ Bi ₂ Br ₉ | 437 | Blue | 65 | 52 | NCs | 208 |
| | MA ₃ Bi ₂ Br ₉ | 430 | Blue | 62 | 12 | NCs | 209 |
| MA ₃ Bi ₂ (Cl, Br) ₉ | 422 | Blue | 41 | 54.1^a | NCs | 210 | |

^aThe highest value of PLQY for each category of Pb-free perovskites, as highlighted in a bold font.

In the same objective of reducing the use of fossil fuel, the CO₂ reduction has also a very important role to play and it has witnessed significant progress by using perovskite materials. For instance, in 2017, Xu *et al.*²²⁴ used CsPbBr₃ nanocrystals (NCs) as novel photocatalysts for CO₂ reduction at a rate of 23.73 μmol g⁻¹ h⁻¹ and up to 29.78 μmol g⁻¹ h⁻¹, with graphene oxide to collect the charge of the CsPbBr₃ NCs. Although Pb-based perovskites are potential candidates for photocatalysts, they are also somehow limited by their low chemical stability.

To ensure the long-term stability of photocathode and photoanode and to avoid Pb contamination during the pre- and post-processing, Pb-free perovskites have been investigated as alternative solutions.¹⁹ Among the technical specifications for an effective photocatalyst, a relatively wide optical bandgap lying in the visible range is ideal for promoting the photocatalytic reaction. Therefore, double perovskites and the 2D perovskite derivatives are of particular interest for such applications. In addition, the high ambient stabilities of these Pb-free materials, compared to conventional 3D perovskites (and especially with respect to Sn²⁺ compounds) makes them even more promising. In fact, first-principles calculations²²⁵ predict that most of the Bi/Ag double perovskites have both bandgaps and energy levels that are suitable for photocatalytic water splitting. On the other hand, in order to promote the CO₂ reduction reaction, further chemical engineering is needed to tune the bandgaps of double as well as 2D layered perovskites. For example, the synthesized all-inorganic Pb-free double perovskite Cs₂AgBiX₆ NCs have their indirect bandgaps decreasing from 2.56 eV when X = Cl to 1.82 eV when X = I.²²⁶ As a result, the Cs₂AgBiI₆ NCs shows the best photoreduction activity with a CO yield of 18.9 μmol g⁻¹ under visible light irradiation (λ ≥ 420 nm, 300 W Xe lamp) within 3 h. Similarly, the bandgap of the 2D layered perovskite Cs₃Bi₂X₉ NCs decreases from 3.08 to 2.01 eV as halide X goes from Cl⁻ to I⁻.²²⁷ The highest CO yielding speed is 54 μmol·g⁻¹ when X = Br_{0.5}I_{0.5}, compared to the 48 μmol g⁻¹ when X = Cl_{0.5}Br_{0.5} and 11 μmol g⁻¹ when X = I under visible-light irradiation (λ ≥ 420 nm, 300 W Xe lamp) for 3 h. The suitable band structure, wide light absorption range, large photocurrent, and small impedance of Cs₃Bi₂(Br_{0.5}I_{0.5})₉ contribute to its greater activity in gas–solid interface than in the majority of the liquid-phase CO₂ reduction systems.

Table III lists photocatalytic applications of different types of Pb-free perovskites and the yielding speed (in μmol g⁻¹ h⁻¹) concerning CO₂ reduction into CO and/or CH₄ and H₂ evolution. In double perovskites, the Cs₂AgBiBr₆ nanoplatelets show the best performance for CO₂ reduction.²²⁸ Within 6 h, these nanoplatelets have a total electron consumption eightfold higher than that of Cs₂AgBiBr₆ NCs, namely, 255.4 vs 30.8 μmol g⁻¹. This large increase can be explained by the anisotropic confinement of charge carriers and the in-plane long diffusion length in nanoplatelets.^{229–231} In order to further improve H₂ production, Jiang *et al.*²³² have synthesized successfully a composite of Cs₂AgBiBr₆ supported on nitrogen-doped carbon materials (N–C). This heterostructure Cs₂AgBiBr₆/N–C has a speed almost 20-fold faster than the pure Cs₂AgBiBr₆. In 2D layered perovskite photocatalysts, their surface activities are strongly dominated by the defects/traps. For example, the Cs₃Sb₂Br₉ NCs exhibit the highest CO yield of 127.5 μmol g⁻¹ h⁻¹ to date.²³³ One explanation is the existence of Sb on their surfaces, which leads to a great improvement of the reactivity. This is in contrast to the nonreactive surfaces of the Pb based perovskites.

Although 3D perovskites are not the most popular for photocatalytic applications, several breakthroughs are still made by using the high hydrophobic dimethylammonium (DMA = CH₃NH₂CH₃⁺) as the A site cation. In 2021, Romani *et al.*²³⁴ have successfully integrated DMASnX₃ with the graphitic carbon nitride (g-C₃N₄), forming the DMASnBr₃@g-C₃N₄. Thanks to the efficient transport of charge carriers, its highest rate of H₂ production in deionized water reaches 1730 μmol g⁻¹ h⁻¹, which is much higher than the 6.0 μmol g⁻¹ h⁻¹ of pure DMASnBr₃ and 2.0 μmol g⁻¹ h⁻¹ of pure g-C₃N₄. The small differences in interfacial energy between CBM of DMASnBr₃ and H⁺/H₂ reduction potential and between VBM of g-C₃N₄ and triethanolamine oxidation potential are proposed to contribute to a large nonadiabatic charge transfer between DMASnBr₃ and g-C₃N₄,²³⁵ and in turn the high photocatalytic yield.

It should be mentioned that apart from the CO₂ reduction reaction and H₂ production, the double and 2D layered perovskites also show potential for more complex reactions involving the transformation of one molecule into another (for clarity they are not listed in Table III).²³⁶ For example, the Cs₂AgBiBr₆ NCs can degrade 97% of toxic NO gas within 30 min and maintain stability in four

TABLE III. Overview of the various Pb-free halide perovskites used for photocatalytic applications. Boldface denotes state of the art results.

| Category | Compounds | Yielding of main product ($\mu\text{mol g}^{-1} \text{h}^{-1}$) | | | Reference |
|--|--|---|---------------------------|-------------------------|-----------|
| | | CO | CH ₄ | H ₂ | |
| ABX ₃ | DMASnI ₃ | | | 0.64 | 240 |
| | DMASnBr ₃ | | | 6 | 241 |
| | DMASnBr ₃ + 10% triethanolamine + 1 wt. % Pt | | | 11 | 241 |
| | DMASnBr ₃ + 10% triethanolamine + 3 wt. % Pt | | | 6 | 234 |
| | DMASnBr ₃ @C ₃ N ₄ -33% + 10% triethanolamine + 3 wt. % Pt | | | 1730^a | 234 |
| A ₂ BB'X ₆ | Cs ₂ AgBiBr ₆ (NCs) | 0.92 | 0.11 | | 242 |
| | Cs ₂ AgBiBr ₆ (washed NCs) | 2.35 | 0.16 | | 242 |
| | Cs ₂ AgBiBr ₆ (bulk) | 0.37 | 0.02 | | 242 |
| | Cs ₂ AgBiI ₆ (NCs) | 6.3 | | | 226 |
| | Cs ₂ AgBi(Br _{0.5} I _{0.5}) ₆ (NCs) | 3.93 | | | 226 |
| | Cs ₂ AgBiCl ₆ (NCs) | 4.54 | | | 226 |
| | Cs ₂ AgBiBr ₆ @C ₃ N ₄ -10% | ~1.8 | ~0.2 | | 243 |
| | Cs ₂ AgBiBr ₆ @C ₃ N ₄ -82% | ~0.66 | ~1.54 | | 243 |
| | Cs ₂ AgBiBr ₆ (nanocubes) | 3.8 | 1.3 | | 228 |
| | Cs ₂ AgBiBr ₆ (nanoplatelets) | 28.1^a | 14.5^a | | 228 |
| | Cs ₂ AgBiBr ₆ /N-C | | | 380^a | 232 |
| | Cs ₂ AgBiBr ₆ | | | 20 | 232 |
| | Cs ₂ AgBiBr ₆ /RGO | | | 48.9 | 244 |
| | Cs ₂ AgBiBr ₆ (bulk) | | | 0.077 | 245 |
| | Cs ₂ AgBiBr ₆ (defect-rich) | | | 0.406 | 245 |
| Cs ₂ AgBiBr ₆ /Pt | | | 0.733 | 245 | |
| Cs ₂ AgBiBr ₆ /Mo ₃ S ₁₃ ²⁻ | | | 2.47 | 245 | |
| A ₃ B ₂ X ₉ | Cs ₃ Sb ₂ Br ₉ | 127.5^a | | | 233 |
| | Cs ₃ Sb ₂ I ₉ (microblocks) | 2.4 | | | 246 |
| | Cs ₃ Sb ₂ I ₉ (microclusters) | 1.7 | | | 246 |
| | Cs ₃ Sb ₂ I ₉ | 92.8 | 2.9 | 10.4 | 247 |
| | Cs ₃ Bi ₂ Cl ₉ | 21.01 | | | 248 |
| | Cs ₃ Bi ₂ Br ₉ | 26.95 | | | 248 |
| | Cs ₃ Bi ₂ (Br _{0.5} I _{0.5}) ₉ | 18 | | | 227 |
| | Cs ₃ Bi ₂ (Cl _{0.5} Br _{0.5}) ₉ | 16 | | | 227 |
| | Cs ₃ Bi ₂ I ₉ | 7.76 | 1.49 | | 249 |
| | Rb ₃ Bi ₂ I ₉ | 1.82 | 1.70 | | 249 |
| | MA ₃ Bi ₂ I ₉ | 0.72 | 0.98 | | 249 |
| | Cs ₃ Bi ₂ I ₉ (QDs) | | | 32.21 | 250 |
| | Cs ₃ Bi ₂ I ₉ @NH ₂ -UiO-66 | | | 141.87 | 250 |
| MA ₃ Bi ₂ I ₉ | | | 169.21^a | 251 | |
| Cs ₃ Bi _{0.6} Sb _{1.4} I ₉ | | | 926 | 252 | |

^aThe highest value of product yielding rate for each category of Pb-free perovskites, as highlighted in a bold font.

runs of photocatalytic reaction.²³⁷ An almost complete degradation (~98%) of Rhodamine B is obtained by Cs₂AgBiBr₆ photocatalysis during 120 min under continuous irradiation.²³⁸ Cs₂AgInCl₆ particles degrade ~98.5% of the water-insoluble carcinogen Sudan Red III in just 16 min and have good stability for five cycle operations.²³⁶ In 2020, (MA_xCs_{1-x})₃SbBr₉ was used for the first time for the activation of C-H bonds, with improved photocatalytic performance, thanks to the substitution of MA by Cs.²³⁹ This unique effect of the A site cation tuning is proposed to stem from the octahedron distortion

induced by the A cation, which changes not only the electronic properties of the X anions but also the electron transfer from molecules to Br sites.

The summary of various types of Pb-free materials employed so far for photo-catalytic applications is further reported in Fig. 2(c). Double (45%) and 2D layered perovskites (41%) are predominant. The remaining 14% are conventional single ABX₃ Pb-free halide perovskites that have been solely used for the photocatalysis of H₂. Obviously, vacancy ordered Pb-free halide perovskites have not yet

been explored for photocatalysis. In the conventional and double perovskites, all the B site cations are Sn and Ag–Bi, respectively. Instead, in 2D layered perovskites, 66% of the explored site B cations are based on pure Bi, 27% on pure Sb, and the remaining 7% on a mixture of both cations. As the material needs to absorb visible light efficiently, metal halides based on Br (54%) and I (33%) are most often used for photocatalytic applications. As for LEDs, most of the A site cations employed in Pb-free perovskites used as photocatalysts are inorganic (81%). To be noted, compositions with mixed organic-inorganic A site cations have not been reported so far.

VI. CONCLUSION

This Perspective reports on the state-of-the-art of Pb-free halide perovskite semiconductors for optoelectronic applications, focusing on solar cells, LEDs, and photocatalysts. Clearly, Sn-based halide perovskites are the most explored and performant for photovoltaic applications. On the other hand, Bi, Ag, and Sb atoms are predominant in the composition of photocatalysts, whereas for LEDs many more metallic cations have been explored with the prevalence of alloys.

For solar cell applications, the PCE achieved to date for any of the double perovskites $A_2BB'X_6$, vacancy ordered double perovskites A_2BX_6 , or 2D perovskite derivatives $A_3B_2X_9$ is below 4% and thus far away from the 25.8% achieved with Pb-based halide perovskites.¹⁰ Tin-iodides $ASnI_3$ compositions are the most promising with a current record reaching 14.6%.⁷⁹ They also allow room for improvements given that the predicted theoretical limit for thick layers under AM1.5G illumination for stannates is as high as 32.3%.⁸³ The materials are less stable than their Pb-based counterparts when subjected to ambient conditions due to the fast Sn^{2+} oxidation. Yet, a remarkable improvement was achieved recently with over 1300 h of operational stability in N_2 , thanks to chemical engineering by combining the addition of a secondary ammonium salt with that of an effective reducing agent.⁸⁰ In addition, Sn/Ge mixed perovskite absorbers also demonstrate improved stability, but their PCE needs to be significantly enhanced. Noteworthy, due to their low electronic bandgap, the Sn-based iodide perovskites can become cornerstone materials and pave the way for tandem perovskite/perovskite solar cells or applications based on low bandgaps.^{253,254}

For LED applications, Pb-free halide perovskite materials, in particular, $A_2BB'X_6$ double perovskite and A_2BX_6 vacancy ordered double perovskite show great promise, especially for white light emission. Indeed, their PLQYs for the white color emission are higher than 78% and those for other colors are remarkably high with some of them higher than 93%. More precisely, 93% for the green emission when $B = In/Sb$ mixture and $B' = K$ in $A_2BB'X_6$ and 95.4% for the yellow–green emission when $B = Sn/Te$ mixture in A_2BX_6 . Noteworthy, these attractive PLQYs are just one of many features needed to make efficient LEDs. Interface related issues are anticipated to be one of the key factors that limit the potential of lead-free perovskites for photovoltaic applications.

Finally, the Pb-free halide double perovskites and 2D layered perovskites are also promising in the field of photocatalysis due to their large electronic bandgap and stability.²¹¹ For instance, Zhou *et al.* synthesized $Cs_2AgBiBr_6$ nanocrystals that were shown to be stable for more than three weeks in a low polarity medium under

light-soaking and 55% relative humidity.²⁴² Double perovskites with $B = Bi$ and $B' = Ag$ have the highest rate of H_2 evolution that reaches $380 \mu\text{mol g}^{-1} \text{h}^{-1}$ when supported on carbon doped with nitrogen.²³² More recently, an impressive hydrogen evolution rate over $1700 \mu\text{mol g}^{-1} \text{h}^{-1}$ was achieved with the use of the ABX_3 $DMASnBr_3$ and $g\text{-C}_3\text{N}_4$, thanks to the favorable alignment of the interfacial energy levels. Regarding CO_2 reduction, the highest rate reported so far with Pb-free halide perovskite catalysts amounts to $127.5 \mu\text{mol g}^{-1} \text{h}^{-1}$ and uses the layered $Cs_3Sb_2Br_9$ material. This type of development is still in its infancy and Pb-free metal halide perovskites show great potential as catalytically active materials, especially in the form of nanocrystals such as nanoplatelets, which offer desirable features such as exposed facets.

ACKNOWLEDGMENTS

This project received funding from the European Union's Horizon 2020 Research and Innovation Program [Grant Agreement Nos. 862656 (DROP-IT) and 861985 (PeroCUBE)]. G.V. acknowledges funding from the Chaire de Recherche Rennes Metropole project. J.E. acknowledges financial support from the Institut Universitaire de France.

AUTHOR DECLARATIONS

Conflict of Interest

The authors have no conflicts to disclose.

DATA AVAILABILITY

The data that support the findings of this study are available within the article.

REFERENCES

- 1 S. D. Stranks and H. J. Snaith, *Nat. Nanotechnol.* **10**, 391 (2015).
- 2 M. A. Green, A. Ho-Baillie, and H. J. Snaith, *Nat. Photonics* **8**, 506 (2014).
- 3 K. Lin, J. Xing, L. N. Quan, F. P. G. de Arquer, X. Gong, J. Lu, L. Xie, W. Zhao, D. Zhang, C. Yan, W. Li, X. Liu, Y. Lu, J. Kirman, E. H. Sargent, Q. Xiong, and Z. Wei, *Nature* **562**, 245 (2018).
- 4 K. S. Schanze, P. V. Kamat, P. Yang, and J. Bisquert, *ACS Energy Lett.* **5**, 2602 (2020).
- 5 A. Kojima, K. Teshima, Y. Shirai, and T. Miyasaka, *J. Am. Chem. Soc.* **131**, 6050 (2009).
- 6 S. De Wolf, J. Holovsky, S.-J. Moon, P. Löper, B. Niesen, M. Ledinsky, F.-J. Haug, J.-H. Yum, and C. Ballif, *J. Phys. Chem. Lett.* **5**, 1035 (2014).
- 7 S. D. Stranks, G. E. Eperon, G. Grancini, C. Menelaou, M. J. P. Alcocer, T. Leijtens, L. M. Herz, A. Petrozza, and H. J. Snaith, *Science* **342**, 341 (2013).
- 8 D. Shi, V. Adinolfi, R. Comin, M. Yuan, E. Alarousu, A. Buin, Y. Chen, S. Hoogland, A. Rothenberger, K. Katsiev, Y. Losovyj, X. Zhang, P. A. Dowben, O. F. Mohammed, E. H. Sargent, and O. M. Bakr, *Science* **347**, 519 (2015).
- 9 M. Abdi-Jalebi, Z. Andaji-Garmaroudi, S. Cacovich, C. Stavrakas, B. Philippe, J. M. Richter, M. Alsari, E. P. Booker, E. M. Hutter, A. J. Pearson, S. Lilliu, T. J. Savenije, H. Rensmo, G. Divitini, C. Ducati, R. H. Friend, and S. D. Stranks, *Nature* **555**, 497 (2018).
- 10 H. Min, D. Y. Lee, J. Kim, G. Kim, K. S. Lee, J. Kim, M. J. Paik, Y. K. Kim, K. S. Kim, M. G. Kim, T. J. Shin, and S. Il Seok, *Nature* **598**, 444 (2021).
- 11 A. Babayigit, A. Ethirajan, M. Muller, and B. Conings, *Nat. Mater.* **15**, 247 (2016).

- ¹²S.-Y. Bae, S. Y. Lee, J.-w. Kim, H. N. Umh, J. Jeong, S. Bae, J. Yi, Y. Kim, and J. Choi, *Sci. Rep.* **9**, 4242 (2019).
- ¹³J. Li, H.-L. Cao, W.-B. Jiao, Q. Wang, M. Wei, I. Cantone, J. Lü, and A. Abate, *Nat. Commun.* **11**, 310 (2020).
- ¹⁴C. Ponti, G. Nasti, D. Di Girolamo, I. Cantone, F. A. Alharthi, and A. Abate, *Trends Ecol. Evol.* **37**, 281 (2022).
- ¹⁵A. Exrance, *Nature* **570**, 429 (2019).
- ¹⁶T. A. Berhe, W.-N. Su, C.-H. Chen, C.-J. Pan, J.-H. Cheng, H.-M. Chen, M.-C. Tsai, L.-Y. Chen, A. A. Dubale, and B.-J. Hwang, *Energy Environ. Sci.* **9**, 323 (2016).
- ¹⁷J. S. Manser, M. I. Saidaminov, J. A. Christians, O. M. Bakr, and P. V. Kamat, *Acc. Chem. Res.* **49**, 330 (2016).
- ¹⁸W. Ke, C. C. Stoumpos, and M. G. Kanatzidis, *Adv. Mater.* **31**, 1803230 (2019).
- ¹⁹C. Pareja-Rivera, D. Morett, D. Barreiro-Argüelles, P. Olalde-Velasco, and D. Solis-Ibarra, *J. Phys. Energy* **3**, 032014 (2021).
- ²⁰Q. A. Akkerman and L. Manna, *ACS Energy Lett.* **5**, 604 (2020).
- ²¹S. Boyer-Richard, C. Katan, B. Traoré, R. Scholz, J.-M. Jancu, and J. Even, *J. Phys. Chem. Lett.* **7**, 3833 (2016).
- ²²I. Chung, J.-H. Song, J. Im, J. Androulakis, C. D. Malliakas, H. Li, A. J. Freeman, J. T. Kenney, and M. G. Kanatzidis, *J. Am. Chem. Soc.* **134**, 8579 (2012).
- ²³C. C. Stoumpos, C. D. Malliakas, and M. G. Kanatzidis, *Inorg. Chem.* **52**, 9019 (2013).
- ²⁴F. Hao, C. C. Stoumpos, D. H. Cao, R. P. H. Chang, and M. G. Kanatzidis, *Nat. Photonics* **8**, 489 (2014).
- ²⁵N. K. Noel, S. D. Stranks, A. Abate, C. Wehrenfennig, S. Guarnera, A.-A. Haghighirad, A. Sadhanala, G. E. Eperon, S. K. Pathak, M. B. Johnston, A. Petrozza, L. M. Herz, and H. J. Snaith, *Energy Environ. Sci.* **7**, 3061 (2014).
- ²⁶S. Gupta, D. Cahen, and G. Hodes, *J. Phys. Chem. C* **122**, 13926 (2018).
- ²⁷X. Meng, Y. Wang, J. Lin, X. Liu, X. He, J. Barbaud, T. Wu, T. Noda, X. Yang, and L. Han, *Joule* **4**, 902 (2020).
- ²⁸A. Kaltzoglou, G. K. Manolis, M. M. Elsenety, I. Koutselas, V. Psycharis, A. G. Kontos, and P. Falaras, *J. Electron. Mater.* **48**, 7533 (2019).
- ²⁹W. Ke, C. C. Stoumpos, M. Zhu, L. Mao, I. Spanopoulos, J. Liu, O. Y. Kontsevoi, M. Chen, D. Sarma, Y. Zhang, M. R. Wasielewski, and M. G. Kanatzidis, *Sci. Adv.* **3**, e1701293 (2017).
- ³⁰C. C. Stoumpos, L. Frazer, D. J. Clark, Y. S. Kim, S. H. Rhim, A. J. Freeman, J. B. Ketterson, J. I. Jang, and M. G. Kanatzidis, *J. Am. Chem. Soc.* **137**, 6804 (2015).
- ³¹G. E. Eperon, T. Leijtens, K. A. Bush, R. Prasanna, T. Green, J. T.-W. Wang, D. P. McMeehin, G. Volonakis, R. L. Milot, R. May, A. Palmstrom, D. J. Slotcavage, R. A. Belisle, J. B. Patel, E. S. Parrott, R. J. Sutton, W. Ma, F. Moghadam, B. Conings, A. Babayigit, H.-G. Boyen, S. Bent, F. Giustino, L. M. Herz, M. B. Johnston, M. D. McGehee, and H. J. Snaith, *Science* **354**, 861 (2016).
- ³²M. Chen, M.-G. Ju, H. F. Garces, A. D. Carl, L. K. Ono, Z. Hawash, Y. Zhang, T. Shen, Y. Qi, R. L. Grimm, D. Pacifici, X. C. Zeng, Y. Zhou, and N. P. Padture, *Nat. Commun.* **10**, 16 (2019).
- ³³S. Shao, J. Liu, G. Portale, H.-H. Fang, G. R. Blake, G. H. ten Brink, L. J. A. Koster, and M. A. Loi, *Adv. Energy Mater.* **8**, 1702019 (2017).
- ³⁴J. Dong, S. Shao, S. Kahmann, A. J. Rommens, D. Hermida-Merino, G. H. ten Brink, M. A. Loi, and G. Portale, *Adv. Funct. Mater.* **30**, 2001294 (2020).
- ³⁵C. W. Cross and W. F. Hillebrand, *Am. J. Sci.* **s3-26**, 271 (1883).
- ³⁶A. H. Slavney, T. Hu, A. M. Lindenberg, and H. I. Karunadasa, *J. Am. Chem. Soc.* **138**, 2138 (2016).
- ³⁷E. T. McClure, M. R. Ball, W. Windl, and P. M. Woodward, *Chem. Mater.* **28**, 1348 (2016).
- ³⁸G. Volonakis, M. R. Filip, A. A. Haghighirad, N. Sakai, B. Wenger, H. J. Snaith, and F. Giustino, *J. Phys. Chem. Lett.* **7**, 1254 (2016).
- ³⁹G. Volonakis, A. A. Haghighirad, R. L. Milot, W. H. Sio, M. R. Filip, B. Wenger, M. B. Johnston, L. M. Herz, H. J. Snaith, and F. Giustino, *J. Phys. Chem. Lett.* **8**, 772 (2017).
- ⁴⁰A. H. Slavney, L. Leppert, A. Saldivar Valdes, D. Bartesaghi, T. J. Savenije, J. B. Neaton, and H. I. Karunadasa, *Angew. Chem., Int. Ed.* **57**, 12765 (2018).
- ⁴¹G. Volonakis, A. A. Haghighirad, H. J. Snaith, and F. Giustino, *J. Phys. Chem. Lett.* **8**, 3917 (2017).
- ⁴²F. Wei, Z. Deng, S. Sun, N. T. P. Hartono, H. L. Seng, T. Buonassisi, P. D. Bristowe, and A. K. Cheetham, *Chem. Commun.* **55**, 3721 (2019).
- ⁴³F. Wei, Z. Deng, S. Sun, F. Xie, G. Kieslich, D. M. Evans, M. A. Carpenter, P. D. Bristowe, and A. K. Cheetham, *Mater. Horiz.* **3**, 328 (2016).
- ⁴⁴M. R. Filip, S. Hillman, A. A. Haghighirad, H. J. Snaith, and F. Giustino, *J. Phys. Chem. Lett.* **7**, 2579 (2016).
- ⁴⁵B. A. Connor, R.-I. Biega, L. Leppert, and H. I. Karunadasa, *Chem. Sci.* **11**, 7708 (2020).
- ⁴⁶Z. Deng, F. Wei, S. Sun, G. Kieslich, A. K. Cheetham, and P. D. Bristowe, *J. Mater. Chem. A* **4**, 12025 (2016).
- ⁴⁷A. H. Slavney, L. Leppert, D. Bartesaghi, A. Gold-Parker, M. F. Toney, T. J. Savenije, J. B. Neaton, and H. I. Karunadasa, *J. Am. Chem. Soc.* **139**, 5015 (2017).
- ⁴⁸G. Volonakis, N. Sakai, H. J. Snaith, and F. Giustino, *J. Phys. Chem. Lett.* **10**, 1722 (2019).
- ⁴⁹E. A. Pogue, J. Bond, C. Imperato, J. B. S. Abraham, N. Drichko, and T. M. McQueen, *J. Am. Chem. Soc.* **143**, 19033 (2021).
- ⁵⁰B. Vargas, E. Ramos, E. Pérez-Gutiérrez, J. C. Alonso, and D. Solis-Ibarra, *J. Am. Chem. Soc.* **139**, 9116 (2017).
- ⁵¹B. Vargas, G. Rodríguez-López, and D. Solis-Ibarra, *ACS Energy Lett.* **5**, 3591 (2020).
- ⁵²M. Liu, S. K. Matta, H. Ali-Löyty, A. Matuhina, G. K. Grandhi, K. Lahtonen, S. P. Russo, and P. Vivo, *Nano Lett.* **22**, 311 (2022).
- ⁵³B. Vargas, D. T. Reyes-Castillo, E. Coutino-Gonzalez, C. Sánchez-Aké, C. Ramos, C. Falcony, and D. Solis-Ibarra, *Chem. Mater.* **32**, 9307 (2020).
- ⁵⁴W. L. Hong, P. H. Lo, H. Z. Chiu, S. F. Horng, and Y. C. Chao, *Adv. Mater. Interfaces* **8**, 2002240 (2021).
- ⁵⁵S. Ullah, J. Wang, M. H. Alvi, R. Chang, P. Yang, L. Liu, S. E. Yang, T. Xia, H. Guo, and Y. Chen, *Int. J. Energy Res.* **45**, 1720 (2021).
- ⁵⁶B. Lee, C. C. Stoumpos, N. Zhou, F. Hao, C. Malliakas, C.-Y. Yeh, T. J. Marks, M. G. Kanatzidis, and R. P. H. Chang, *J. Am. Chem. Soc.* **136**, 15379 (2014).
- ⁵⁷A. E. Maughan, A. M. Ganose, M. M. Bordelon, E. M. Miller, D. O. Scanlon, and J. R. Neilson, *J. Am. Chem. Soc.* **138**, 8453 (2016).
- ⁵⁸N. Sakai, A. A. Haghighirad, M. R. Filip, P. K. Nayak, S. Nayak, A. Ramadan, Z. Wang, F. Giustino, and H. J. Snaith, *J. Am. Chem. Soc.* **139**, 6030 (2017).
- ⁵⁹Q. Mahmood, M. Hassan, N. Yousaf, A. A. AlObaid, T. I. Al-Muhimeed, M. Morsi, H. Albalawi, and O. A. Alamri, *Mater. Sci. Semicond. Process.* **137**, 106180 (2022).
- ⁶⁰H. A. Evans, D. H. Fabini, J. L. Andrews, M. Koerner, M. B. Preefer, G. Wu, F. Wudl, A. K. Cheetham, and R. Seshadri, *Inorg. Chem.* **57**, 10375 (2018).
- ⁶¹C. Wu, F. Guo, L. Zhuang, X. Ai, F. Zhong, H. Yang, and J. Qian, *ACS Energy Lett.* **5**, 1644 (2020).
- ⁶²B. Cucco, G. Boudier, L. Pedesseau, C. Katan, J. Even, M. Kepenekian, and G. Volonakis, *Appl. Phys. Lett.* **119**, 181903 (2021).
- ⁶³J. Zhang, Y. Yang, H. Deng, U. Farooq, X. Yang, J. Khan, J. Tang, and H. Song, *ACS Nano* **11**, 9294 (2017).
- ⁶⁴F. Lazarini, *Acta Crystallogr., Sect. B: Struct. Crystallogr. Cryst. Chem.* **33**, 2961 (1977).
- ⁶⁵A. V. Arakcheeva, M. Bonin, G. Chapuis, and A. I. Zaitsev, *Z. Kristallogr. - Cryst. Mater.* **214**, 279 (1999).
- ⁶⁶B. Chabot and E. Parthé, *Acta Crystallogr., Sect. B: Struct. Crystallogr. Cryst. Chem.* **34**, 645 (1978).
- ⁶⁷K. Yamada, H. Sera, S. Sawada, H. Tada, T. Okuda, and H. Tanaka, *J. Solid State Chem.* **134**, 319 (1997).
- ⁶⁸S.-Y. Kim, Y. Yun, S. Shin, J. H. Lee, Y.-W. Heo, and S. Lee, *Scr. Mater.* **166**, 107 (2019).
- ⁶⁹M. Xia, J. H. Yuan, G. Niu, X. Du, L. Yin, W. Pan, J. Luo, Z. Li, H. Zhao, K. H. Xue, X. Miao, and J. Tang, *Adv. Funct. Mater.* **30**, 1910648 (2020).
- ⁷⁰B. Lee, J. He, R. P. Chang, and M. G. Kanatzidis, *Nature* **485**, 486 (2012).
- ⁷¹M. M. Lee, J. Teuscher, T. Miyasaka, T. N. Murakami, and H. J. Snaith, *Science* **338**, 643 (2012).
- ⁷²H.-S. Kim, C.-R. Lee, J.-H. Im, K.-B. Lee, T. Moehl, A. Marchioro, S.-J. Moon, R. Humphry-Baker, J.-H. Yum, J. E. Moser, M. Grätzel, and N.-G. Park, *Sci. Rep.* **2**, 591 (2012).
- ⁷³P. Tockhorn, J. Sutter, A. Cruz, P. Wagner, K. Jäger, D. Yoo, F. Lang, M. Grischek, B. Li, A. Al-Ashouri, E. Köhnen, M. Stollerfoht, D. Neher, R. Schlattmann, B. Rech, B. Stannowski, S. Albrecht, and C. Becker, "Nano-optical

- designs enhance monolithic perovskite/silicon tandem solar cells toward 29.8% efficiency," *Nat. Portfolio* (published online) (2022).
- ⁷⁴H. Tsai, W. Nie, J.-C. Blancon, C. C. Stoumpos, R. Asadpour, B. Harutyunyan, A. J. Neukirch, R. Verduzco, J. J. Crochet, S. Tretiak, L. Pedesseau, J. Even, M. A. Alam, G. Gupta, J. Lou, P. M. Ajayan, M. J. Bedzyk, M. G. Kanatzidis, and A. D. Mohite, *Nature* **536**, 312 (2016).
- ⁷⁵L. Mao, C. C. Stoumpos, and M. G. Kanatzidis, *J. Am. Chem. Soc.* **141**, 1171 (2018).
- ⁷⁶K. Nishimura, M. A. Kamarudin, D. Hirotani, K. Hamada, Q. Shen, S. Iikubo, T. Minemoto, K. Yoshino, and S. Hayase, *Nano Energy* **74**, 104858 (2020).
- ⁷⁷T. Ye, X. Wang, K. Wang, S. Ma, D. Yang, Y. Hou, J. Yoon, K. Wang, and S. Priya, *ACS Energy Lett.* **6**, 1480 (2021).
- ⁷⁸C. Wang, Y. Zhang, F. Gu, Z. Zhao, H. Li, H. Jiang, Z. Bian, and Z. Liu, *Matter* **4**, 709 (2021).
- ⁷⁹X. Jiang, H. Li, Q. Zhou, Q. Wei, M. Wei, L. Jiang, Z. Wang, Z. Peng, F. Wang, Z. Zang, K. Xu, Y. Hou, S. Teale, W. Zhou, R. Si, X. Gao, E. H. Sargent, and Z. Ning, *J. Am. Chem. Soc.* **143**, 10970 (2021).
- ⁸⁰J. Sanchez-Diaz, R. S. Sánchez, S. Masi, M. Krečmarová, A. O. Alvarez, E. M. Barea, J. Rodriguez-Romero, V. S. Chirvony, J. F. Sánchez-Royo, J. P. Martínez-Pastor, and I. Mora-Seró, *Joule* **6**, 861 (2022).
- ⁸¹L.-J. Chen, C.-R. Lee, Y.-J. Chuang, Z.-H. Wu, and C. Chen, *J. Phys. Chem. Lett.* **7**, 5028 (2016).
- ⁸²P. Wang, F. Li, K. J. Jiang, Y. Zhang, H. Fan, Y. Zhang, Y. Miao, J. H. Huang, C. Gao, X. Zhou, F. Wang, L. M. Yang, C. Zhan, and Y. Song, *Adv. Sci.* **7**, 1903047 (2020).
- ⁸³A. Filippetti, S. Kahmann, C. Caddeo, A. Mattoni, M. Saba, A. Bosin, and M. A. Loi, *J. Mater. Chem. A* **9**, 11812 (2021).
- ⁸⁴B. Li, H. Di, B. Chang, R. Yin, L. Fu, Y. N. Zhang, and L. Yin, *Adv. Funct. Mater.* **31**, 2007447 (2021).
- ⁸⁵E. Jökar, C.-H. Chien, C.-M. Tsai, A. Fathi, and E. W.-G. Diau, *Adv. Mater.* **31**, 1804835 (2019).
- ⁸⁶Q. Zeng, X. Zhang, X. Feng, S. Lu, Z. Chen, X. Yong, S. A. T. Redfern, H. Wei, H. Wang, H. Shen, W. Zhang, W. Zheng, H. Zhang, J. S. Tse, and B. Yang, *Adv. Mater.* **30**, 1705393 (2018).
- ⁸⁷F. Li, C. Zhang, J. H. Huang, H. Fan, H. Wang, P. Wang, C. Zhan, C. M. Liu, X. Li, L. M. Yang, Y. Song, and K. J. Jiang, *Angew. Chem., Int. Ed.* **58**, 6688 (2019).
- ⁸⁸F. Hao, C. C. Stoumpos, R. P. H. Chang, and M. G. Kanatzidis, *J. Am. Chem. Soc.* **136**, 8094 (2014).
- ⁸⁹T.-B. Song, T. Yokoyama, C. C. Stoumpos, J. Logsdon, D. H. Cao, M. R. Wasielewski, S. Aramaki, and M. G. Kanatzidis, *J. Am. Chem. Soc.* **139**, 836 (2017).
- ⁹⁰F. Hao, C. C. Stoumpos, P. Guo, N. Zhou, T. J. Marks, R. P. H. Chang, and M. G. Kanatzidis, *J. Am. Chem. Soc.* **137**, 11445 (2015).
- ⁹¹T. Fujihara, S. Terakawa, T. Matsushima, C. Qin, M. Yahiro, and C. Adachi, *J. Mater. Chem. C* **5**, 1121 (2017).
- ⁹²T. Handa, T. Yamada, H. Kubota, S. Ise, Y. Miyamoto, and Y. Kanemitsu, *J. Phys. Chem. C* **121**, 16158 (2017).
- ⁹³T. Yokoyama, D. H. Cao, C. C. Stoumpos, T.-B. Song, Y. Sato, S. Aramaki, and M. G. Kanatzidis, *J. Phys. Chem. Lett.* **7**, 776 (2016).
- ⁹⁴M.-C. Jung, S. R. Raga, and Y. Qi, *RSC Adv.* **6**, 2819 (2016).
- ⁹⁵E. Greul, P. Docampo, and T. Bein, *Z. Anorg. Allg. Chem.* **643**, 1704 (2017).
- ⁹⁶C.-M. Tsai, N. Mohanta, C.-Y. Wang, Y.-P. Lin, Y.-W. Yang, C.-L. Wang, C.-H. Hung, and E. W.-G. Diau, *Angew. Chem.* **129**, 14007 (2017).
- ⁹⁷T. Yokoyama, T.-B. Song, D. H. Cao, C. C. Stoumpos, S. Aramaki, and M. G. Kanatzidis, *ACS Energy Lett.* **2**, 22 (2017).
- ⁹⁸X. Liu, Z. Yang, C.-C. Chueh, A. Rajagopal, S. T. Williams, Y. Sun, and A. K.-Y. Jen, *J. Mater. Chem. A* **4**, 17939 (2016).
- ⁹⁹Z. Zhang, L. Wang, A. Kumar Baranwal, S. Razyeh Sahamir, G. Kapil, Y. Sanehira, M. Akmal Kamarudin, K. Nishimura, C. Ding, D. Liu, Y. Li, H. Li, M. Chen, Q. Shen, T. S. Ripolles, J. Bisquert, and S. Hayase, *J. Energy Chem.* **71**, 604 (2022).
- ¹⁰⁰X. Jiang, F. Wang, Q. Wei, H. Li, Y. Shang, W. Zhou, C. Wang, P. Cheng, Q. Chen, L. Chen, and Z. Ning, *Nat. Commun.* **11**, 1245 (2020).
- ¹⁰¹M. Chen, Q. Dong, F. T. Eickemeyer, Y. Liu, Z. Dai, A. D. Carl, B. Bahrami, A. H. Chowdhury, R. L. Grimm, Y. Shi, Q. Qiao, S. M. Zakeeruddin, M. Grätzel, and N. P. Padture, *ACS Energy Lett.* **5**, 2223 (2020).
- ¹⁰²T. Wu, X. Liu, X. He, Y. Wang, X. Meng, T. Noda, X. Yang, and L. Han, *Sci. China Chem.* **63**, 107 (2020).
- ¹⁰³F. Gu, S. Ye, Z. Zhao, H. Rao, Z. Liu, Z. Bian, and C. Huang, *Sol. RRL* **2**, 1800136 (2018).
- ¹⁰⁴Z. Zhao, F. Gu, Y. Li, W. Sun, S. Ye, H. Rao, Z. Liu, Z. Bian, and C. Huang, *Adv. Sci.* **4**, 1700204 (2017).
- ¹⁰⁵X. Meng, J. Lin, X. Liu, X. He, Y. Wang, T. Noda, T. Wu, X. Yang, and L. Han, *Adv. Mater.* **31**, 1903721 (2019).
- ¹⁰⁶W. Liao, D. Zhao, Y. Yu, C. R. Grice, C. Wang, A. J. Cimaroli, P. Schulz, W. Meng, K. Zhu, R. G. Xiong, and Y. Yan, *Adv. Mater.* **28**, 9333 (2016).
- ¹⁰⁷W. Ke, C. C. Stoumpos, J. L. Logsdon, M. R. Wasielewski, Y. Yan, G. Fang, and M. G. Kanatzidis, *J. Am. Chem. Soc.* **138**, 14998 (2016).
- ¹⁰⁸J. Xi, Z. Wu, B. Jiao, H. Dong, C. Ran, C. Piao, T. Lei, T. B. Song, W. Ke, T. Yokoyama, X. Hou, and M. G. Kanatzidis, *Adv. Mater.* **29**, 1606964 (2017).
- ¹⁰⁹T. M. Koh, T. Krishnamoorthy, N. Yantara, C. Shi, W. L. Leong, P. P. Boix, A. C. Grimsdale, S. G. Mhaisalkar, and N. Mathews, *J. Mater. Chem. A* **3**, 14996 (2015).
- ¹¹⁰W. Gu, X. Xu, J. Chen, B. Ma, M. Qin, W. Zhu, J. Qian, Z. Qin, W. Shen, Y. Lu, W. Zhang, S. Chen, X. Lu, and W. Huang, *Sol. RRL* **4**, 2000153 (2020).
- ¹¹¹S. J. Lee, S. S. Shin, J. Im, T. K. Ahn, J. H. Noh, N. J. Jeon, S. I. Seok, and J. Seo, *ACS Energy Lett.* **3**, 46 (2017).
- ¹¹²X. Liu, K. Yan, D. Tan, X. Liang, H. Zhang, and W. Huang, *ACS Energy Lett.* **3**, 2701 (2018).
- ¹¹³J. Liu, M. Ozaki, S. Yakumar, T. Handa, R. Nishikubo, Y. Kanemitsu, A. Saeki, Y. Murata, R. Murdey, and A. Wakamiya, *Angew. Chem.* **130**, 13405 (2018).
- ¹¹⁴N. Ito, M. A. Kamarudin, D. Hirotani, Y. Zhang, Q. Shen, Y. Ogomi, S. Iikubo, T. Minemoto, K. Yoshino, and S. Hayase, *J. Phys. Chem. Lett.* **9**, 1682 (2018).
- ¹¹⁵C. H. Ng, K. Nishimura, N. Ito, K. Hamada, D. Hirotani, Z. Wang, F. Yang, S. Iikubo, Q. Shen, K. Yoshino, T. Minemoto, and S. Hayase, *Nano Energy* **58**, 130 (2019).
- ¹¹⁶T.-B. Song, T. Yokoyama, S. Aramaki, and M. G. Kanatzidis, *ACS Energy Lett.* **2**, 897 (2017).
- ¹¹⁷T.-B. Song, T. Yokoyama, J. Logsdon, M. R. Wasielewski, S. Aramaki, and M. G. Kanatzidis, *ACS Appl. Energy Mater.* **1**, 4221 (2018).
- ¹¹⁸K. Marshall, M. Walker, R. Walton, and R. Hatton, *Nat. Energy* **1**, 16178 (2016).
- ¹¹⁹N. Wang, Y. Zhou, M.-G. Ju, H. F. Garces, T. Ding, S. Pang, X. C. Zeng, N. P. Padture, and X. W. Sun, *Adv. Energy Mater.* **6**, 1601130 (2016).
- ¹²⁰K. P. Marshall, R. I. Walton, and R. A. Hatton, *J. Mater. Chem. A* **3**, 11631 (2015).
- ¹²¹M. H. Kumar, S. Dharani, W. L. Leong, P. P. Boix, R. R. Prabhakar, T. Baikie, C. Shi, H. Ding, R. Ramesh, M. Asta, M. Graetzel, S. G. Mhaisalkar, and N. Mathews, *Adv. Mater.* **26**, 7122 (2014).
- ¹²²W. Li, J. Li, J. Li, J. Fan, Y. Mai, and L. Wang, *J. Mater. Chem. A* **4**, 17104 (2016).
- ¹²³S. Gupta, T. Bendikov, G. Hodes, and D. Cahen, *ACS Energy Lett.* **1**, 1028 (2016).
- ¹²⁴D. Moghe, L. Wang, C. J. Traverse, A. Redoute, M. Sponseller, P. R. Brown, V. Bulović, and R. R. Lunt, *Nano Energy* **28**, 469 (2016).
- ¹²⁵I. Kopacic, B. Friesenbichler, S. F. Hoefler, B. Kunert, H. Plank, T. Rath, and G. Trimmel, *ACS Appl. Energy Mater.* **1**, 343 (2018).
- ¹²⁶L.-J. Chen, *RSC Adv.* **8**, 18396 (2018).
- ¹²⁷T. Krishnamoorthy, H. Ding, C. Yan, W. L. Leong, T. Baikie, Z. Zhang, M. Sherburne, S. Li, M. Asta, N. Mathews, and S. G. Mhaisalkar, *J. Mater. Chem. A* **3**, 23829 (2015).
- ¹²⁸W. Ke, C. C. Stoumpos, I. Spanopoulos, L. Mao, M. Chen, M. R. Wasielewski, and M. G. Kanatzidis, *J. Am. Chem. Soc.* **139**, 14800 (2017).
- ¹²⁹B. Wang, N. Li, L. Yang, C. Dall'Agnese, A. K. Jena, S. Sasaki, T. Miyasaka, H. Tamiaki, and X.-F. Wang, *J. Am. Chem. Soc.* **143**, 2207 (2021).
- ¹³⁰X. Yang, Y. Chen, P. Liu, H. Xiang, W. Wang, R. Ran, W. Zhou, and Z. Shao, *Adv. Funct. Mater.* **30**, 2001557 (2020).
- ¹³¹E. Greul, M. L. Petrus, A. Binek, P. Docampo, and T. Bein, *J. Mater. Chem. A* **5**, 19972 (2017).
- ¹³²C. Wu, Q. Zhang, Y. Liu, W. Luo, X. Guo, Z. Huang, H. Ting, W. Sun, X. Zhong, S. Wei, S. Wang, Z. Chen, and L. Xiao, *Adv. Sci.* **5**, 1700759 (2018).

- ¹³³P.-K. Kung, M.-H. Li, P.-Y. Lin, J.-Y. Jhang, M. Pantaler, D. C. Lupascu, G. Grancini, and P. Chen, *Sol. RRL* **4**, 1900306 (2020).
- ¹³⁴Z. Zhang, C. Wu, D. Wang, G. Liu, Q. Zhang, W. Luo, X. Qi, X. Guo, Y. Zhang, Y. Lao, B. Qu, L. Xiao, and Z. Chen, *Org. Electron.* **74**, 204 (2019).
- ¹³⁵C. Zhang, L. Gao, S. Teo, Z. Guo, Z. Xu, S. Zhao, and T. Ma, *Sustainable Energy Fuels* **2**, 2419 (2018).
- ¹³⁶E. M. Hutter, G. E. Eperon, S. D. Stranks, and T. J. Savenije, *J. Phys. Chem. Lett.* **6**, 3082 (2015).
- ¹³⁷X. Qiu, Y. Jiang, H. Zhang, Z. Qiu, S. Yuan, P. Wang, and B. Cao, *Phys. Status Solidi RRL* **10**, 587 (2016).
- ¹³⁸B. Lee, A. Krenselewski, S. I. Baik, D. N. Seidman, and R. P. H. Chang, *Sustainable Energy Fuels* **1**, 710 (2017).
- ¹³⁹Y. Jiang, H. Zhang, X. Qiu, and B. Cao, *Mater. Lett.* **199**, 50 (2017).
- ¹⁴⁰M. Chen, M.-G. Ju, A. D. Carl, Y. Zong, R. L. Grimm, J. Gu, X. C. Zeng, Y. Zhou, and N. P. Padture, *Joule* **2**, 558 (2018).
- ¹⁴¹A. Kaltzoglou, M. Antoniadou, D. Perganti, E. Siranidi, V. Raptis, K. Trohidou, V. Psycharis, A. G. Kontos, and P. Falaras, *Electrochim. Acta* **184**, 466 (2015).
- ¹⁴²X. Zhang, G. Wu, Z. Gu, B. Guo, W. Liu, S. Yang, T. Ye, C. Chen, W. Tu, and H. Chen, *Nano Res.* **9**, 2921 (2016).
- ¹⁴³C. Ran, Z. Wu, J. Xi, F. Yuan, H. Dong, T. Lei, X. He, and X. Hou, *J. Phys. Chem. Lett.* **8**, 394 (2017).
- ¹⁴⁴S. S. Mali, H. Kim, D.-H. Kim, and C. Kook Hong, *ChemistrySelect* **2**, 1578 (2017).
- ¹⁴⁵A. Kulkarni, T. Singh, M. Ikegami, and T. Miyasaka, *RSC Adv.* **7**, 9456 (2017).
- ¹⁴⁶B.-W. Park, B. Philippe, X. Zhang, H. Rensmo, G. Boschloo, and E. M. J. Johansson, *Adv. Mater.* **27**, 6806 (2015).
- ¹⁴⁷M. Abulikemu, S. Ould-Chikh, X. Miao, E. Alarousu, B. Murali, G. O. Ngongang Ndjawa, J. Barbé, A. El Labban, A. Amassian, and S. Del Gobbo, *J. Mater. Chem. A* **4**, 12504 (2016).
- ¹⁴⁸T. Okano and Y. Suzuki, *Mater. Lett.* **191**, 77 (2017).
- ¹⁴⁹S. Öz, J.-C. Hebig, E. Jung, T. Singh, A. Lepcha, S. Olthof, F. Jan, Y. Gao, R. German, P. H. M. van Loosdrecht, K. Meerholz, T. Kirchartz, and S. Mathur, *Sol. Energy Mater. Sol. Cells* **158**, 195 (2016).
- ¹⁵⁰H. Li, C. Wu, Y. Yan, B. Chi, J. Pu, J. Li, and S. Priya, *ChemSusChem* **10**, 3994 (2017).
- ¹⁵¹P. Karuppuswamy, K. M. Boopathi, A. Mohapatra, H.-C. Chen, K.-T. Wong, P.-C. Wang, and C.-W. Chu, *Nano Energy* **45**, 330 (2018).
- ¹⁵²K. M. Boopathi, P. Karuppuswamy, A. Singh, C. Hanmandlu, L. Lin, S. A. Abbas, C. C. Chang, P. C. Wang, G. Li, and C. W. Chu, *J. Mater. Chem. A* **5**, 20843 (2017).
- ¹⁵³S. Chatterjee and A. J. Pal, *ACS Appl. Mater. Interfaces* **10**, 35194 (2018).
- ¹⁵⁴J.-C. Hebig, I. Kühn, J. Flohre, and T. Kirchartz, *ACS Energy Lett.* **1**, 309 (2016).
- ¹⁵⁵M. B. Johansson, H. Zhu, and E. M. J. Johansson, *J. Phys. Chem. Lett.* **7**, 3467 (2016).
- ¹⁵⁶P. C. Harikesh, H. K. Mulmudi, B. Ghosh, T. W. Goh, Y. T. Teng, K. Thirumal, M. Lockrey, K. Weber, T. M. Koh, S. Li, S. Mhaisalkar, and N. Mathews, *Chem. Mater.* **28**, 7496 (2016).
- ¹⁵⁷C. Zuo and L. Ding, *Angew. Chem.* **129**, 6628 (2017).
- ¹⁵⁸A. Rajagopal, R. J. Stoddard, H. W. Hillhouse, and A. K.-Y. Jen, *J. Mater. Chem. A* **7**, 16285 (2019).
- ¹⁵⁹T. Luo, Y. Xia, J. Huang, X. Huang, Z. Wu, Y. Chen, X. Xu, W. Xie, P. Liu, C. Hu, X. Lu, and T. Shi, *CrystEngComm* **23**, 4917 (2021).
- ¹⁶⁰J. Chang, L. Jiang, G. Wang, W. Zhao, Y. Huang, and H. Chen, *Phys. Chem. Chem. Phys.* **23**, 14449 (2021).
- ¹⁶¹Y. Raoui, S. Kazim, Y. Galagan, H. Ez-Zahraouy, and S. Ahmad, *Sustainable Energy Fuels* **5**, 4661 (2021).
- ¹⁶²L. Schade, S. Mahesh, G. Volonakis, M. Zacharias, B. Wenger, F. Schmidt, S. V. Kesava, D. Prabhakaran, M. Abdi-Jalebi, M. Lenz, F. Giustino, G. Longo, P. G. Radaelli, and H. J. Snaith, *ACS Energy Lett.* **6**, 1073 (2021).
- ¹⁶³Q. Zhou, Z. Bai, W.-g. Lu, Y. Wang, B. Zou, and H. Zhong, *Adv. Mater.* **28**, 9163 (2016).
- ¹⁶⁴C. Cho, B. Zhao, G. D. Tainter, J.-Y. Lee, R. H. Friend, D. Di, F. Deschler, and N. C. Greenham, *Nat. Commun.* **11**, 611 (2020).
- ¹⁶⁵Z. Liu, W. Qiu, X. Peng, G. Sun, X. Liu, D. Liu, Z. Li, F. He, C. Shen, Q. Gu, F. Ma, H. L. Yip, L. Hou, Z. Qi, and S. J. Su, *Adv. Mater.* **33**, 2103268 (2021).
- ¹⁶⁶H. Tsai, S. Shrestha, R. A. Vilá, W. Huang, C. Liu, C.-H. Hou, H.-H. Huang, X. Wen, M. Li, G. Wiederrecht, Y. Cui, M. Cotlet, X. Zhang, X. Ma, and W. Nie, *Nat. Photonics* **15**, 843 (2021).
- ¹⁶⁷Y. Dong, Y.-K. Wang, F. Yuan, A. Johnston, Y. Liu, D. Ma, M.-J. Choi, B. Chen, M. Chekini, S.-W. Baek, L. K. Sagar, J. Fan, Y. Hou, M. Wu, S. Lee, B. Sun, S. Hoogland, R. Quintero-Bermudez, H. Ebe, P. Todorovic, F. Dinic, P. Li, H. T. Kung, M. I. Saidaminov, E. Kumacheva, E. Spiecker, L.-S. Liao, O. Voznyy, Z.-H. Lu, and E. H. Sargent, *Nat. Nanotechnol.* **15**, 668 (2020).
- ¹⁶⁸Z. Zhu, Y. Wu, Y. Shen, J. Tan, D. Shen, M.-F. Lo, M. Li, Y. Yuan, J.-X. Tang, W. Zhang, S.-W. Tsang, Z. Guan, and C.-S. Lee, *Chem. Mater.* **33**, 4154 (2021).
- ¹⁶⁹H. Xiang, R. Wang, J. Chen, F. Li, and H. Zeng, *Light: Sci. Appl.* **10**, 206 (2021).
- ¹⁷⁰R. Sun, P. Lu, D. Zhou, W. Xu, N. Ding, H. Shao, Y. Zhang, D. Li, N. Wang, X. Zhuang, B. Dong, X. Bai, and H. Song, *ACS Energy Lett.* **5**, 2131 (2020).
- ¹⁷¹K. Zhang, N. Zhu, M. Zhang, L. Wang, and J. Xing, *J. Mater. Chem. C* **9**, 3795 (2021).
- ¹⁷²L. Protesescu, S. Yakunin, M. I. Bodnarchuk, F. Krieg, R. Caputo, C. H. Hendon, R. X. Yang, A. Walsh, and M. V. Kovalenko, *Nano Lett.* **15**, 3692 (2015).
- ¹⁷³Y.-H. Kim, H. Cho, J. H. Heo, T.-S. Kim, N. Myoung, C.-L. Lee, S. H. Im, and T.-W. Lee, *Adv. Mater.* **27**, 1248 (2015).
- ¹⁷⁴J. Song, J. Li, X. Li, L. Xu, Y. Dong, and H. Zeng, *Adv. Mater.* **27**, 7162 (2015).
- ¹⁷⁵B. Ke, R. Zeng, Z. Zhao, Q. Wei, X. Xue, K. Bai, C. Cai, W. Zhou, Z. Xia, and B. Zou, *J. Phys. Chem. Lett.* **11**, 340 (2020).
- ¹⁷⁶P. Han, X. Mao, S. Yang, F. Zhang, B. Yang, D. Wei, W. Deng, and K. Han, *Angew. Chem.* **131**, 17391 (2019).
- ¹⁷⁷J. Luo, X. Wang, S. Li, J. Liu, Y. Guo, G. Niu, L. Yao, Y. Fu, L. Gao, Q. Dong, C. Zhao, M. Leng, F. Ma, W. Liang, L. Wang, S. Jin, J. Han, L. Zhang, J. Etheridge, J. Wang, Y. Yan, E. H. Sargent, and J. Tang, *Nature* **563**, 541 (2018).
- ¹⁷⁸K. z. Du, W. Meng, X. Wang, Y. Yan, and D. B. Mitzi, *Angew. Chem., Int. Ed.* **56**, 8158 (2017).
- ¹⁷⁹T. T. Tran, J. R. Panella, J. R. Chamorro, J. R. Morey, and T. M. McQueen, *Mater. Horiz.* **4**, 688 (2017).
- ¹⁸⁰F. Locardi, M. Cirignano, D. Baranov, Z. Dang, M. Prato, F. Drago, M. Ferretti, V. Pinchetti, M. Fanciulli, S. Brovelli, L. De Trizio, and L. Manna, *J. Am. Chem. Soc.* **140**, 12989 (2018).
- ¹⁸¹J. D. Majher, M. B. Gray, T. A. Strom, and P. M. Woodward, *Chem. Mater.* **31**, 1738 (2019).
- ¹⁸²C.-Y. Wang, P. Liang, R.-J. Xie, Y. Yao, P. Liu, Y. Yang, J. Hu, L. Shao, X. W. Sun, F. Kang, and G. Wei, *Chem. Mater.* **32**, 7814 (2020).
- ¹⁸³M. Hu, J. Luo, S. Li, J. Liu, J. Li, Z. Tan, G. Niu, Z. Wang, and J. Tang, *Opt. Lett.* **44**, 4757 (2019).
- ¹⁸⁴G. Zhou, X. Jiang, M. Molokeev, Z. Lin, J. Zhao, J. Wang, and Z. Xia, *Chem. Mater.* **31**, 5788 (2019).
- ¹⁸⁵A. Nocolak, V. Morad, K. M. McCall, S. Yakunin, Y. Shynkarenko, M. Wörle, and M. V. Kovalenko, *Chem. Mater.* **32**, 5118 (2020).
- ¹⁸⁶Z. Tan, Y. Chu, J. Chen, J. Li, G. Ji, G. Niu, L. Gao, Z. Xiao, and J. Tang, *Adv. Mater.* **32**, 2002443 (2020).
- ¹⁸⁷Z. Li, C. Zhang, B. Li, C. Lin, Y. Li, L. Wang, and R.-J. Xie, *Chem. Eng. J.* **420**, 129740 (2021).
- ¹⁸⁸A. Wang, Y. Guo, F. Muhammad, and Z. Deng, *Chem. Mater.* **29**, 6493 (2017).
- ¹⁸⁹A. B. Wong, Y. Bekenstein, J. Kang, C. S. Kley, D. Kim, N. A. Gibson, D. Zhang, Y. Yu, S. R. Leone, L.-W. Wang, A. P. Alivisatos, and P. Yang, *Nano Lett.* **18**, 2060 (2018).
- ¹⁹⁰F. Yuan, J. Xi, H. Dong, K. Xi, W. Zhang, C. Ran, B. Jiao, X. Hou, A. K.-Y. Jen, and Z. Wu, *Phys. Status Solidi RRL* **12**, 1800090 (2018).
- ¹⁹¹W.-L. Hong, Y.-C. Huang, C.-Y. Chang, Z.-C. Zhang, H.-R. Tsai, N.-Y. Chang, and Y.-C. Chao, *Adv. Mater.* **28**, 8029 (2016).
- ¹⁹²Z. Yang, Z. Jiang, X. Liu, X. Zhou, J. Zhang, and W. Li, *Adv. Opt. Mater.* **7**, 1900108 (2019).
- ¹⁹³B. Yang, J. Chen, S. Yang, F. Hong, L. Sun, P. Han, T. Pullerits, W. Deng, and K. Han, *Angew. Chem.* **130**, 5457 (2018).
- ¹⁹⁴S. Li, Q. Hu, J. Luo, T. Jin, J. Liu, J. Li, Z. Tan, Y. Han, Z. Zheng, T. Zhai, H. Song, L. Gao, G. Niu, and J. Tang, *Adv. Opt. Mater.* **7**, 1901098 (2019).

- ¹⁹⁵P. Han, X. Zhang, X. Mao, B. Yang, S. Yang, Z. Feng, D. Wei, W. Deng, T. Pullerits, and K. Han, *Sci. China Chem.* **62**, 1405 (2019).
- ¹⁹⁶F. Locardi, E. Sartori, J. Buha, J. Zito, M. Prato, V. Pinchetti, M. L. Zaffalon, M. Ferretti, S. Brovelli, I. Infante, L. De Trizio, and L. Manna, *ACS Energy Lett.* **4**, 1976 (2019).
- ¹⁹⁷A. Karmakar, G. M. Bernard, A. Meldrum, A. O. Oliynyk, and V. K. Michaelis, *J. Am. Chem. Soc.* **142**, 10780 (2020).
- ¹⁹⁸F. Zhao, Z. Song, J. Zhao, and Q. Liu, *Inorg. Chem. Front.* **6**, 3621 (2019).
- ¹⁹⁹K. N. Nandha and A. Nag, *Chem. Commun.* **54**, 5205 (2018).
- ²⁰⁰Q. Hu, Z. Deng, M. Hu, A. Zhao, Y. Zhang, Z. Tan, G. Niu, H. Wu, and J. Tang, *Sci. China Chem.* **61**, 1581 (2018).
- ²⁰¹Z. Tan, J. Li, C. Zhang, Z. Li, Q. Hu, Z. Xiao, T. Kamiya, H. Hosono, G. Niu, E. Lifshitz, Y. Cheng, and J. Tang, *Adv. Funct. Mater.* **28**, 1801131 (2018).
- ²⁰²J. Li, Z. Tan, M. Hu, C. Chen, J. Luo, S. Li, L. Gao, Z. Xiao, G. Niu, and J. Tang, *Front. Optoelectron.* **12**, 352 (2019).
- ²⁰³H. Zhang, L. Zhu, J. Cheng, L. Chen, C. Liu, and S. Yuan, *Materials* **12**, 1501 (2019).
- ²⁰⁴B. M. Benin, D. N. Dirin, V. Morad, M. Wörle, S. Yakunin, G. Rainò, O. Nazarenko, M. Fischer, I. Infante, and M. V. Kovalenko, *Angew. Chem., Int. Ed.* **57**, 11329 (2018).
- ²⁰⁵G. Xiong, L. Yuan, Y. Jin, H. Wu, Z. Li, B. Qu, G. Ju, L. Chen, S. Yang, and Y. Hu, *Adv. Opt. Mater.* **8**, 2000779 (2020).
- ²⁰⁶M. Leng, Y. Yang, K. Zeng, Z. Chen, Z. Tan, S. Li, J. Li, B. Xu, D. Li, M. P. Hautzinger, Y. Fu, T. Zhai, L. Xu, G. Niu, S. Jin, and J. Tang, *Adv. Funct. Mater.* **28**, 1704446 (2018).
- ²⁰⁷Z. Ma, Z. Shi, D. Yang, F. Zhang, S. Li, L. Wang, D. Wu, Y. Zhang, G. Na, L. Zhang, X. Li, Y. Zhang, and C. Shan, *ACS Energy Lett.* **5**, 385 (2020).
- ²⁰⁸Y. Shen, J. Yin, B. Cai, Z. Wang, Y. Dong, X. Xu, and H. Zeng, *Nanoscale Horiz.* **5**, 580 (2020).
- ²⁰⁹M. Leng, Z. Chen, Y. Yang, Z. Li, K. Zeng, K. Li, G. Niu, Y. He, Q. Zhou, and J. Tang, *Angew. Chem., Int. Ed.* **55**, 15012 (2016).
- ²¹⁰M. Leng, Y. Yang, Z. Chen, W. Gao, J. Zhang, G. Niu, D. Li, H. Song, J. Zhang, S. Jin, and J. Tang, *Nano Lett.* **18**, 6076 (2018).
- ²¹¹E. Gong, S. Ali, C. B. Hiragond, H. S. Kim, N. S. Powar, D. Kim, H. Kim, and S.-I. In, *Energy Environ. Sci.* **15**, 880 (2022).
- ²¹²K. Ren, S. Yue, C. Li, Z. Fang, K. A. M. Gasem, J. Leszczynski, S. Qu, Z. Wang, and M. Fan, *J. Mater. Chem. A* **10**, 407 (2022).
- ²¹³S. Purohit, K. L. Yadav, and S. Satapathi, *Adv. Mater. Interfaces* **9**, 2200058 (2022).
- ²¹⁴H. Huang, B. Weng, H. Zhang, F. Lai, J. Long, J. Hofkens, R. E. Douthwaite, J. A. Steele, and M. B. J. Roeffaers, *J. Phys. Chem. Lett.* **13**, 25 (2022).
- ²¹⁵O. Khaselev and J. A. Turner, *Science* **280**, 425 (1998).
- ²¹⁶M. M. May, H.-J. Lewerenz, D. Lackner, F. Dimroth, and T. Hannappel, *Nat. Commun.* **6**, 8286 (2015).
- ²¹⁷J. Jia, L. C. Seitz, J. D. Benck, Y. Huo, Y. Chen, J. W. D. Ng, T. Bilir, J. S. Harris, and T. F. Jaramillo, *Nat. Commun.* **7**, 13237 (2016).
- ²¹⁸W.-H. Cheng, M. H. Richter, M. M. May, J. Ohlmann, D. Lackner, F. Dimroth, T. Hannappel, H. A. Atwater, and H.-J. Lewerenz, *ACS Energy Lett.* **3**, 1795 (2018).
- ²¹⁹J. Tournet, Y. Lee, S. K. Karuturi, H. H. Tan, and C. Jagadish, *ACS Energy Lett.* **5**, 611 (2020).
- ²²⁰J. Gao, F. Sahli, C. Liu, D. Ren, X. Guo, J. Werner, Q. Jeangros, S. M. Zakeeruddin, C. Ballif, M. Grätzel, and J. Luo, *Joule* **3**, 2930 (2019).
- ²²¹S. Park, W. J. Chang, C. W. Lee, S. Park, H.-Y. Ahn, and K. T. Nam, *Nat. Energy* **2**, 16185 (2017).
- ²²²X. Wang, H. Wang, H. Zhang, W. Yu, X. Wang, Y. Zhao, X. Zong, and C. Li, *ACS Energy Lett.* **3**, 1159 (2018).
- ²²³H. Wang, X. Wang, R. Chen, H. Zhang, X. Wang, J. Wang, J. Zhang, L. Mu, K. Wu, F. Fan, X. Zong, and C. Li, *ACS Energy Lett.* **4**, 40 (2019).
- ²²⁴Y.-F. Xu, M.-Z. Yang, B.-X. Chen, X.-D. Wang, H.-Y. Chen, D.-B. Kuang, and C.-Y. Su, *J. Am. Chem. Soc.* **139**, 5660 (2017).
- ²²⁵G. Volonakis and F. Giustino, *Appl. Phys. Lett.* **112**, 243901 (2018).
- ²²⁶D. Wu, X. Zhao, Y. Huang, J. Lai, H. Li, J. Yang, C. Tian, P. He, Q. Huang, and X. Tang, *Chem. Mater.* **33**, 4971 (2021).
- ²²⁷D. Wu, X. Zhao, Y. Huang, J. Lai, J. Yang, C. Tian, P. He, Q. Huang, and X. Tang, *J. Phys. Chem. C* **125**, 18328 (2021).
- ²²⁸Z. Liu, H. Yang, J. Wang, Y. Yuan, K. Hills-Kimball, T. Cai, P. Wang, A. Tang, and O. Chen, *Nano Lett.* **21**, 1620 (2021).
- ²²⁹G. Zhang, A. Chaves, S. Huang, F. Wang, Q. Xing, T. Low, and H. Yan, *Sci. Adv.* **4**, eaap9977 (2018).
- ²³⁰T. Otterburg, D. Y. Oberli, M.-A. Dupertuis, N. Moret, E. Pelucchi, B. Dwir, K. Leifer, and E. Kapon, *Phys. Rev. B* **71**, 033301 (2005).
- ²³¹K. Zheng, Q. Zhu, M. Abdellah, M. E. Messing, W. Zhang, A. Generalov, Y. Niu, L. Ribaud, S. E. Canton, and T. Pullerits, *J. Phys. Chem. Lett.* **6**, 2969 (2015).
- ²³²Y. Jiang, K. Li, X. Wu, M. Zhu, H. Zhang, K. Zhang, Y. Wang, K. P. Loh, Y. Shi, and Q.-H. Xu, *ACS Appl. Mater. Interfaces* **13**, 10037 (2021).
- ²³³C. Lu, D. S. Itanze, A. G. Aragon, X. Ma, H. Li, K. B. Ucer, C. Hewitt, D. L. Carroll, R. T. Williams, Y. Qiu, and S. M. Geyer, *Nanoscale* **12**, 2987 (2020).
- ²³⁴L. Romani, A. Speltini, F. Ambrosio, E. Mosconi, A. Profumo, M. Marelli, S. Margadonna, A. Milella, F. Fracassi, A. Listorti, F. De Angelis, and L. Malavasi, *Angew. Chem., Int. Ed.* **60**, 3611 (2021).
- ²³⁵Y. Q. Gao, Y. Georgievskii, and R. A. Marcus, *J. Chem. Phys.* **112**, 3358 (2000).
- ²³⁶K. Li, S. Li, W. Zhang, Z. Shi, D. Wu, X. Chen, P. Lin, Y. Tian, and X. Li, *J. Colloid Interface Sci.* **596**, 376 (2021).
- ²³⁷D. Wu, Y. Tao, Y. Huang, B. Huo, X. Zhao, J. Yang, X. Jiang, Q. Huang, F. Dong, and X. Tang, *J. Catal.* **397**, 27 (2021).
- ²³⁸Z. Zhang, Y. Liang, H. Huang, X. Liu, Q. Li, L. Chen, and D. Xu, *Angew. Chem., Int. Ed.* **58**, 7263 (2019).
- ²³⁹Z. Zhang, Y. Yang, Y. Wang, L. Yang, Q. Li, L. Chen, and D. Xu, *Angew. Chem.* **132**, 18293 (2020).
- ²⁴⁰D. Ju, X. Zheng, J. Liu, Y. Chen, J. Zhang, B. Cao, H. Xiao, O. F. Mohammed, O. M. Bakr, and X. Tao, *Angew. Chem.* **130**, 15084 (2018).
- ²⁴¹A. Pisanu, A. Speltini, P. Quadrelli, G. Drera, L. Sangaletti, and L. Malavasi, *J. Mater. Chem. C* **7**, 7020 (2019).
- ²⁴²L. Zhou, Y.-F. Xu, B.-X. Chen, D.-B. Kuang, and C.-Y. Su, *Small* **14**, 1703762 (2018).
- ²⁴³Y. Wang, H. Huang, Z. Zhang, C. Wang, Y. Yang, Q. Li, and D. Xu, *Appl. Catal., B* **282**, 119570 (2021).
- ²⁴⁴T. Wang, D. Yue, X. Li, and Y. Zhao, *Appl. Catal., B* **268**, 118399 (2020).
- ²⁴⁵Z. He, Q. Tang, X. Liu, X. Yan, K. Li, and D. Yue, *Energy Fuels* **35**, 15005 (2021).
- ²⁴⁶Y. Hai, W. Huang, Z. Li, D. Wu, Q. Huang, and X. Tang, *ACS Appl. Energy Mater.* **4**, 5913 (2021).
- ²⁴⁷Y. Wang, Q. Zhou, Y. Zhu, and D. Xu, *Appl. Catal., B* **294**, 120236 (2021).
- ²⁴⁸J. Sheng, Y. He, J. Li, C. Yuan, H. Huang, S. Wang, Y. Sun, Z. Wang, and F. Dong, *ACS Nano* **14**, 13103 (2020).
- ²⁴⁹S. S. Bhosale, A. K. Kharade, E. Jocar, A. Fathi, S.-m. Chang, and E. W.-G. Diau, *J. Am. Chem. Soc.* **141**, 20434 (2019).
- ²⁵⁰Y.-Y. Wang, X.-Y. Ji, M. Yu, and J. Tao, *Mater. Chem. Front.* **5**, 7796 (2021).
- ²⁵¹Y. Guo, G. Liu, Z. Li, Y. Lou, J. Chen, and Y. Zhao, *ACS Sustainable Chem. Eng.* **7**, 15080 (2019).
- ²⁵²G. Chen, P. Wang, Y. Wu, Q. Zhang, Q. Wu, Z. Wang, Z. Zheng, Y. Liu, Y. Dai, and B. Huang, *Adv. Mater.* **32**, 2001344 (2020).
- ²⁵³J. Tong, Z. Song, D. H. Kim, X. Chen, C. Chen, A. F. Palmstrom, P. F. Ndione, M. O. Reese, S. P. Dunfield, O. G. Reid, J. Liu, F. Zhang, S. P. Harvey, Z. Li, S. T. Christensen, G. Teeter, D. Zhao, M. M. Al-Jassim, M. F. A. M. van Hest, M. C. Beard, S. E. Shaheen, J. J. Berry, Y. Yan, and K. Zhu, *Science* **364**, 475 (2019).
- ²⁵⁴S. R. Sahamir, M. A. Kamarudin, T. S. Ripolles, A. K. Baranwal, G. Kapil, Q. Shen, H. Segawa, J. Bisquert, and S. Hayase, *J. Phys. Chem. Lett.* **13**, 3130 (2022).